Diploma Thesis

Hybrid Model for Static Deformations of Sandwich Beams and its Numerical Validation

submitted in satisfaction of the requirements for the degree of
Diplom-Ingenieur of the TU Wien, Faculty of Mechanical and
Industrial Engineering

Diplomarbeit

Hybridmodell für statische Verformungen von Sandwichträgern und seine numerische Validierung

ausgeführt zum Zwecke der Erlangung des akademischen Grades eines Diplom-Ingenieurs
eingereicht an der Technischen Universität Wien, Fakultät für Maschinenwesen und
Betriebswissenschaften

Matr.Nr.:1229003

Ali Razgordanisharahi BSc.

unter der Anleitung und Betreuung
von

Senior Scientist. Mag. Dr. Yury Vetyukov

Institut für Mechanik und Mechatronik
Forschungsbereich Mechanik fester Körper
Technische Universität Wien
Getreidemarkt 9/E325, 1060 Wien, Österreich

Wien, im April 2021

Ali Razgordanisharahi BSc.

Ich nehme zur Kenntnis, dass ich zur Drucklegung dieser Arbeit unter der Bezeichnung

DIPLOMARBEIT

nur mit Bewilligung der Prüfungskommission berechtigt bin.

Eidesstattliche Erklärung

Ich erkläre an Eid statt, dass die vorliegende Arbeit nach den anerkannten Grundsätzen für wissenschaftliche Abhandlungen von mir selbstständig erstellt wurde. Alle verwendeten Hilfsmittel, insbesondere die zugrunde gelegte Literatur, sind in dieser Arbeit genannt und aufgelistet. Die aus den Quellen wörtlich entnommenen Stellen sind als solche kenntlich gemacht.

Ich nehme zur Kenntnis, dass die vorgelegte Arbeit mit geeigneten und dem derzeitigen Stand der Technik entsprechenden Mitteln (Plagiat-Erkennungssoftware) elektronisch-technisch überprüft wird. Dies stellt einerseits sicher, dass bei der Erstellung der vorgelegten Arbeit die hohen Qualitätsvorgaben im Rahmen der geltenden Regeln zur Sicherung guter wissenschaftlicher Praxis (Code of Conduct) an der TU Wien eingehalten wurden. Zum anderen werden durcheinen Abgleich mit anderen studentischen Abschlussarbeiten Verletzungen meines persönlichen Urheberrechts vermieden.

Wien, im April 2021 Ali Razgordanisharahi BSc.

Kurzfassung

Sandwich-Strukturen haben attraktive Eigenschaften, die in Kombination mit hoher Haltbarkeit und fantastischen Gestaltungsmöglichkeiten einen der wichtigsten Schritte auf dem Weg zu intelligenten Materialien darstellen. In dieser Studie werden die Auswirkungen von Kerndicke und Steifigkeitseigenschaften im Rahmen neuartiger mathematischen Modellierung auf die statische Antwort eines Sandwichträgers auf verteilte Belastung dargestellt. In dieser Arbeit werden vier Berechnungsmethoden verwendet. Drei davon sind numerische Methoden, nämlich ein FEM-Modell mit einem kubischen Funktionsansatz und die Ritz-Methode, eine 2D-Simulation mit ABAQUS. Zusätzlich zu den numerischen Verfahren wird ein äquivalentes einlagiges Balkenmodell betrachtet, um die Ergebnisse des vorgeschlagenen Verbundbalkenmodells zu validieren. Eines der Hauptziele dieser Studie war die Bewertung der Fähigkeit des vorgeschlagenen Verfahrens zur Modellierung des Trägers als einer Kombination von zwei Bernoulli-Euler Balken anstelle von den Deckschichten sowie eines kontinuumsmechanischen Modells des Kerns, genaue Ergebnisse für unterschiedliche Materialeigenschaften der Schichten des Trägers zu finden. Die wichtigste Erkenntnis der Arbeit dreht sich um die Erfassung des Verhaltens des Querschnitts des Trägers durch eine lineare Formulierung. Die Ergebnisse der vorgeschlagenen Methode zeigen eine gute Übereinstimmung mit den ABAQUS-Simulationen als Referenzlösung.

Abstract

Sandwich structures exhibit attractive properties such as high durability and fantastic design capabilities. Owing to their superior mechanical and design capabilities, they are one of the major advancing steps towards intelligent materials. In this study, we aim to investigate the effects of core thickness and stiffness on the static response of a sandwich beam under distributed loading. For this purpose, four methods of analyses are utilized in this thesis. Three of these approaches are numerical methods, namely FEM modeling with cubic interpolation functions, Ritz method and 2D simulation in ABAQUS software. In addition to numerical schemes, an equivalent single layer beam model is considered in order to validate the results of proposed compound beam model. One of the main goals of this study is to evaluate the capacity of the proposed compound method to model the sandwich beam as a combination of two Bernoulli-Euler beams for the face sheets as well as a continuum model of the core in order to find accurate total strain energy of sandwich beams for various material properties of the layers. The most important findings of the current study are related to capturing the behavior of the cross-sections during the deformation in various material parameter ranges. The results of the proposed method stand in a good agreement with the ABAQUS simulations as a reference solution.

Contents

List of figures

List of Table

Chapter 1

Introduction

There is an increasing demand for sandwich structures in aerospace, marine, train, and automobile industries. Therefore, finding an accurate and simple way to analyze the behavior of sandwich structures under different loads seems necessary in this regard. Classical Bernoulli-Euler beam theory, first-order shear deformation theory, multi-dimensional elasticity theory, and finite element analysis are considered as some of the most popular approaches and theories [1-3].

Sandwich beams are widely used in building frames, bridges, cranes, ship hulls, spacecraft, and industrial infrastructures as well as transportation systems. These structures are usually made in the form of assemblies with one or more members and core units with the capability of withstanding a wide range of static and dynamic loads such as shocks, explosions, and forces from sea waves and winds. Moreover, these beams have a structure with a regular and periodic core that will create a good middle ground between performance (energy absorption) and productivity. Accordingly, the core must have an acceptable stiffness in terms of shear forces applied to the structure, which consequently prevents the face sheets from slipping relative to each other. Moreover, the materials used to cover the two surfaces of the structure vary indefinitely. One common material is a face sheet. A plastic core sandwiched between two metallic and thin beams is usually called a double-sided sandwich panel depending on its thickness. One application of this particular sandwich beam is to cover the roof of industrial and workshop sheds. In this type of sandwich panels, the insulations used are typically polyurethane, polystyrene and rock wool. In a double-sided sandwich panel, the thickness of the sheets used must be the same. Otherwise, the heavy sheet will bend towards the lighter sheet.

Lattice and cellular structures have some unique advantages due to their superior strength, modulus, and high adsorption at low densities; therefore, they are used for structures that need to be light-weighted such as airplanes, spacecrafts, and cars. A particular attention in the present thesis is paid to the structure of a sandwich, which consists of two metal face sheets and the core of cellular and lattice materials, combining high energy absorption along with a very lightweight design. The core of the sandwich beam, so they work together in carrying the bending loads. On the other hand, the upper and lower sheets contribute to the tensile stiffness of the beam.

1.1. Composite beams

Beams made of two or more different materials are called composite beams, which are used in thermostats. Plastic-coated tubes and wooden beams with steel reinforcement plates are shown in Figure 1.1 as examples of composite beams.

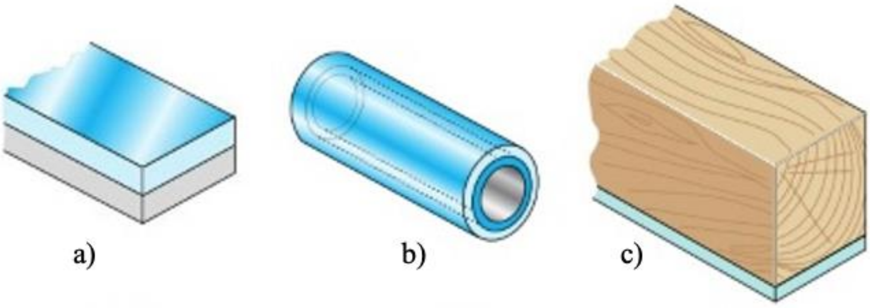

Figure 1.1. Examples of composite beams: a) Bimetallic beams, b) plastic coated pipe, and c) wooden beam with steel reinforcing plates [54].

In recent years, several types of composite beams are used for industrial applications. The main purposes of using these beams are saving the related costs and reducing the weight of structures. Since the use of lightweight components with high strength and rigidity is preferred in lightweight applications of aerospace industry, sandwich beams, as a type of composite beams, are widely used in these applications. Various well-known items such as bookshelves, cardboard boxes, and doors, are also made of sandwich beam structures.

The Figure 1.2 shows some examples of sandwich beams. A typical prototype of this beam consists of two thin face sheets with relatively high strength (such as aluminum plates) as well as a thick core with a relatively lower weight and strength (such as plastic). It is shown that due to the large distance of the plates from the neutral axis (where the most flexural strains occur), their behaviors are similar to those of the wings of an I-shaped beam. The core of the sandwich beam acts as a filler, which provides the necessary support for the plates of the face sheets (this configuration prevents the plates from buckling and wrinkling). Lightweight plastics and foams are mostly used for composite beam cores. In the next section, conventional approaches for analyzing the behavior of composite beams are introduced.

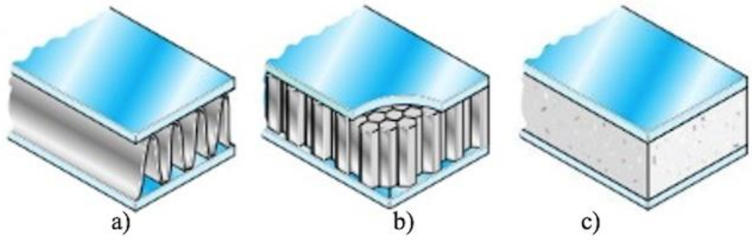

Figure 1.2. Examples of sandwich beams: a) with corrugated core, b) with hive core, and c) with plastic core [54].

1.2. Literature review

The compliance and compressibility of the core in terms of thickness are shown to affect the overall behavior of the sandwich structure and limit the application of theories that cannot model this core behavior [4, 5]. In 1992, a special solution, called the high-order solution of sandwich structures, was proposed by Frostig et al. [6]. Accordingly, in this solution, the sandwich structure was divided into the following three regions: the upper surface, the three-dimensional body of the core, and the lower surface. It was assumed that the upper and lower surfaces follow the classical Bernoulli-Euler beam theory, and the core behavior is governed by three-dimensional elasticity theory. By solving these three regions relative to each other and considering the equations of displacement continuity at the contact point of the core with the sheets, the behavior of the structure was investigated, and the amount of core contraction was then obtained.

One of the advantages of the high-order method is the possibility of applying different boundary conditions on the upper and lower surfaces, as well as considering the contraction and shear effects of the core. Frostig and other researchers in their studies used high-order sandwich theory to investigate the behavior of sandwich structures under different loads with different shapes of beams, sheets, and shells, and under different boundary conditions [6-10].

Thereafter, this theory was gradually upgraded and expanded [11-13]. In order to increase its accuracy in predicting the behavior of sandwich structures, the effect of geometric nonlinearity was also considered [14]. Most of the studies conducted on the nonlinearity of the theory emphasized that only the nonlinear behavior of the sheets can be modeled by considering the kinematic relationships of the sheets based on the von Karman strain [15-16]. The nonlinear behavior of the core was considered in two references [17-18]. In all of them, due to the high complexity, the complete solution of the obtained equations has gone through extensive simplifications.

In addition, the formulation and solution of equations considering large deformations for all the components of the sandwich structure are theoretically of great value; however, these have not been presented by other researchers so far. From an experimental perspective, the linear theories exhibited large errors due to different factors such as the size of the structures, the thinness of the sheets, and the compliance of the core. Due to these limitations and considerations, there is a clear need for a comprehensive consideration of these nonlinear terms.

Taheri-Behrooz et al. [19] investigated the bending behavior of four-point sandwich beams with foam and resin cores as well as different lengths. As a result, it was shown that the mechanisms of destruction of the beams were the depression of the foam and the subsequent failure of the shell in the force application site.

Cone shells are known as one of the most important components of structures applied in the aerospace, civil, and aerospace industries. Lightweight and high force bearing capacities make the broad usage of these structures in various fields of engineering. Cone shells are often subjected to dynamic loads, which makes it particularly important to study their vibrational behaviors. Additionally, the emergence of high-performance composite materials has proposed composite mesh shells as good alternatives to structures reinforced with traditional materials. The reinforced composite structures consist of shells and reinforcements (in the form of beams) that can be placed on both sides of the shells, and then increase the strength and rigidity of the structure significantly without causing any significant increase in weight. Composite lattices simultaneously have the capabilities of both simple composite structures and lattice structures. The properties that led to the widespread use of this type of structure are the ratio of high weight resistance and load-bearing capacity at a limited weight. Sandwich structures are created by the addition of a shell to the reinforced structure, so the reinforcements are placed between the shells. Given the importance of these structures as well as the high cost of performing experimental tests, providing an analytical model with the ability of studying the behavior of these structures under different loads, especially dynamic ones, is of great importance. Most of the previous studies conducted on the mechanical behavior of the reinforced shells have been limited to orthogonal reinforcements, and so far, less research has been devoted to the structures reinforced with diagonal reinforcements (ribs). Accordingly, Kidane et al. [20], by presenting an analytical model of buckling in their study, obtained a continuum model for cylindrical lattice shells with diagonal reinforcements and then compared the results of the analysis with the experimental and numerical results.

The number of applications for sandwich panels is rapidly increasing. The required accuracy in the structural analysis of the panels was found to depend mostly on the type of application considered. For example, in aircrafts, a very detailed response of the sandwich structure may be required, whereas an overall global response may suffice in residential buildings when the natural vibration frequencies are of much interest. In any case, there is a need for proposing appropriate modeling tools for different applications. Reviews on the modeling of sandwich structures have been conducted by several authors [21-25]. Modeling methods for sandwich panels can be classified as follows:

a- Full 3-D analysis (computational or analytical), with complete details of the considered face sheets and the core structure.
b- Layer-wise modeling with the considered faces and core as separate continuum layers [26];
c- Statically equivalent single layer (ESL) models.

Although computational 3-D and layer-wise analyses give very detailed stress distributions for the panels, they come with inherent disadvantages, including large number of variables, and thus, their computational analysis can be very burdensome. Therefore, equivalent single layer theories such as the ESL first-order shear deformation (FSDT) beam and plate models, can be considered as potential alternatives, especially when the global response of the structure is of main interest without accounting for further details. Nowadays, extensive literature exists on the modeling of the sandwich beam, plates, and shells by ESL theories [23, 27-29].

Recently, it was shown that all-steel hive-core sandwich beams deform so that when an ESL-FSDT model is used, the model must take anti-symmetric shear deformations into account for the response of the sandwich structure to be accurately captured in some applications [30].

By the increased interest in micropolar elasticity [31], considerable effort has been devoted to developing appropriate finite element models for micropolar continua in general, for more examples, see [32-35]. To list a few recent finite element models for micropolar plates, the works of Ansari et al. [36, 37] and Godio et al. [38] can be mentioned. Various finite element models have been proposed for the bending analysis of micropolar beams, as well. Huang et al. [39] used 3-D non-compatible finite elements to analyze the bending of beams, and Li and Xie [32] proposed three different elements for plane micropolar elasticity and used them to analyze thin in-plane beams. Hassanpour and Heppler [40] developed a 1-D micropolar beam finite element model using Lagrange interpolation functions. Moreover, Regueiro and Duan [41] derived a finite element model for a micropolar Timoshenko beam with the microrotation, which was assumed to be equal to the cross-sectional rotation. More recently, in another study, Karttunen et al. [30] proposed a nodally-exact 1-D finite element to analyze micropolar Timoshenko beams. In this regard, Ansari et al. [36] proposed a 27-node 3-D finite element for the analysis of beams. It is noteworthy that only linear strains are considered in developing the finite element models in all above-mentioned papers.

1.3. Scientific hypothesis of the present dissertation

In this dissertation, deformation and strain energy of a sandwich beam with a soft core under a static distributed load are investigated using geometrically linear modeling. The novelty of the proposed approach is that thin upper and lower face sheets are modeled as Euler–Bernoulli beams and the core is considered as a two-dimensional continuous body in the state of plane stress that undergoes shear and thickness compression; in the following, we refer to this approach as a *compound model*. The kinematics of deformation of the soft core is fully determined by the bending and axial deformations of the beams. Thus, the deformation of the entire sandwich structure and its strain energy are known as soon as the deformed configurations of the two beams are defined, both with respect to bending and longitudinal stretch. So, the present thesis aims at verifying the accuracy and efficiency of this novel mechanical model of sandwich beams for the possibly broad range of ratios of the stiffness coefficients of the face sheets and the core.

For this purpose, different methods are applied, in order to determine the deformations of a sandwich beam under distributed loading. Along with the proposed compound model, two other models are used for comparison purposes:

- A simple Bernoulli-Euler beam model with an equivalent bending stiffness is considered for validating the compound beam model in order to estimate the material parameter range, in which using the compound model is preferred.
- The full two-dimensional plane stress continuum model of the beam was analyzed using ABAQUS finite element software, which allowed the validation of the proposed method in a broad parameter range as well as estimating the domain of its applicability.

Finally, the simulations in the framework of the proposed compound model are performed using Wolfram Mathematica software via global Ritz approximation and a finite element model. The latter approximations provide degrees of freedom of the upper and lower beams of the sandwich structure. In this work, vectorial and tensorial quantities are represented in a Cartesian coordinate system.

Chapter 2

Problem formulation and simple solution technique

All theories of sandwich beams feature the reduction of the two-dimensional continuous model to a one-dimensional model, which accounts for the particularities of the solution of the plane stress problem of the theory of elasticity for the original structure. In the displacement-based approach, the primary variables are the generalized displacements (displacement, rotation, etc.).

Equivalent Single Layer (ESL) models, also known as Smeared Laminate, are generally based on a smooth expansion (generally as a power series expansion) over the whole laminate thickness of the displacement field in terms of the thickness-wise coordinate. Accordingly, this means that the kinematics along the thickness can be assumed to be at least C1-continuous and independent of the laminate layup. Consequently, the multilayer structure is substituted with a beam composed of an equivalent single layer. Although these are time consuming and also not cost effective, ESL models are not accurate in general, especially when through-the-thickness distribution of strains and stresses are the main concerns, and the laminate is highly heterogeneous. Among the displacement-based ESL models, the most popular ones are the Classical Lamination Plate Theory (CLPT) [42], and the First-order Shear Deformation Theory (FSDT) based on the Timoshenko beam theory [43, 44]. Correspondingly, both CLPT and FSDT make use of a linear expansion of the longitudinal displacement. Besides the weaknesses of the ESL models, it is a well-known fact that FSDT needs ad hoc shear correction factors to yield more accurate results [43-47]. CLPT and FSDT were found to perform relatively well in predicting global quantities such as transverse displacement, fundamental natural frequency, and buckling load for thin and moderately thick laminates with a relatively low degree of transverse heterogeneity. However, their accuracy rapidly diminishes when they are used to predict the displacement and stress fields in highly heterogeneous and/or thick composite as well as sandwich laminates [47, 49-51]. In this regard, the improved predictions can be obtained using higher order through-the-thickness expansions of the displacements and/or stresses [51].

Apart from the equivalent single-layer modeling assumptions, layer-wise theories assume that the behavior of a laminate is determined by an assembly of the individual layers whose kinematic fields are independently described while satisfying some certain physical continuity constraints [48]. It is indicated that the increased kinematic freedom provided by the layer-wise schemes enables the enforcement of the interlaminar stress continuity conditions as well as the modeling of zigzag-like displacement distributions through a laminate thickness. However, the major drawback of such theories is that the number of kinematic variables depends on the number of layers. Therefore, for thick laminates or sandwich structures with a large number of plies, such approaches can be considered as computationally inefficient and particularly cumbersome in order to be implemented within a displacement-based finite element method.

2.1. Dimensions and material properties

A sandwich structured composite is a special class of composite materials fabricated by attaching two thin but stiff skins (face sheets), to a light weight but thick core. The core material is normally made of low strength material, but its higher thickness provides the sandwich composite with high bending stiffness with an overall low density. In this regard, the opened and closed cell-structured foams such as polyvinylchloride, polyurethane, polyethylene or polystyrene foams, and honeycombs are commonly used as core materials. The opened and closed cell metal foam can also be used as core materials. Notably, laminates of glass or carbon fiber reinforced thermoplastics or mainly thermo set polymers (unsaturated polyesters, epoxies, etc.) are widely used as skin materials. Sheet metal can also be used as a skin material in some cases.

There are different types of sandwich structures like metal composite material (MCM), which is a type of sandwich formed from two thin skins of metal bonded to a plastic core during a continuous process under the controlled pressure, heat, and tension. As well, recycled paper is currently being used over a closed cell recycled craft honeycomb core, in order to create a lightweight, strong, and fully repulpable composite board. This material is used due to its applications, including point-of-purchase displays, bulkheads, recyclable office furniture, exhibition stands, and wall dividers. Of note, to fix different panels, a transition zone is normally selected among other solutions. Accordingly, this causes a gradual reduction in the core height, until the two fiber skins will be in touch. In this place, the fixation can be made using bolts, rivets or adhesive. The strength of the composite material depends largely on the following two factors:

- The outer skins or face sheets: If the sandwich is supported on both sides and stressed using a force in the middle of the beam, then the bending moment will introduce shear forces in the material. The core material also spaces these two sheets apart. The thicker the core material, the stronger the composite. This principle works in the same way as an I-beam does.

- The interface between the core and the sheets: Because the shear stresses in the composite material rapidly change between the core and the sheets, the adhesive layer also undergoes some degrees of shear force. If the adhesive bond between the two layers is too weak, delamination is the most probable outcome.

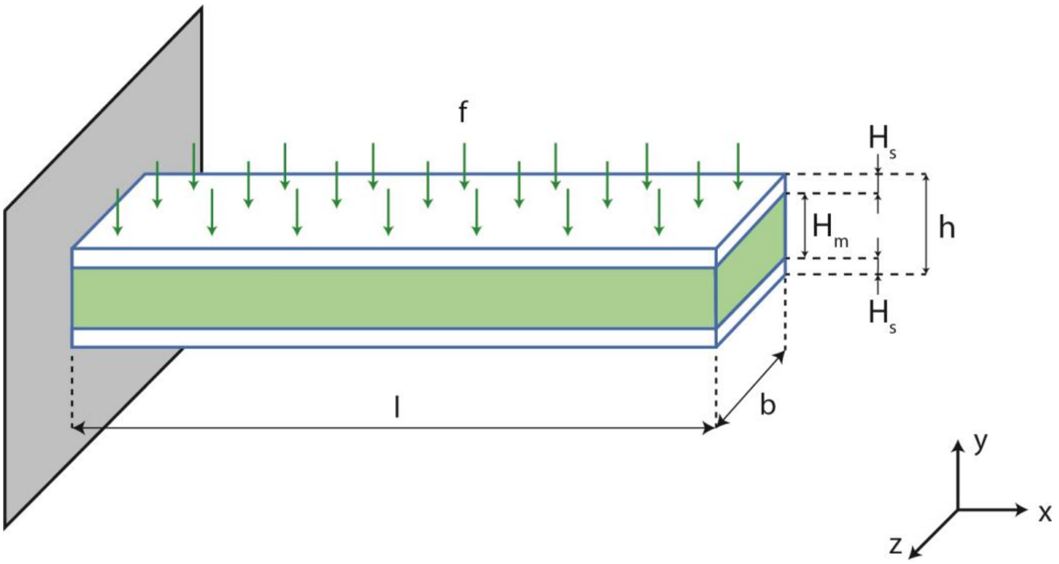

Figure 2.1. The scheme of the considered sandwich beam.

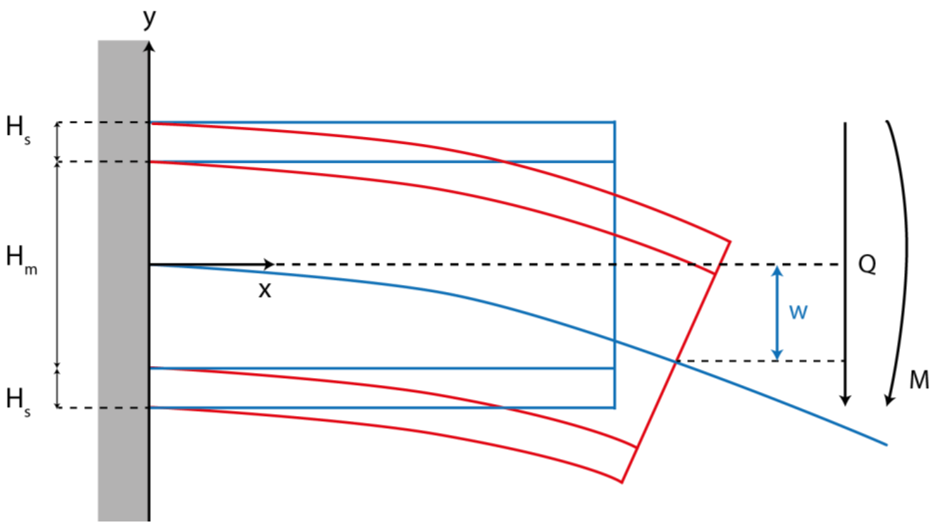

Figure 2.2. Bending of a sandwich beam with no extra deformation due to core shear.

In this study, the upper and lower face sheets are modeled as Euler–Bernoulli beams along with the core as a two-dimensional continuum. Accordingly, the core resists shear, transverse, and longitudinal loads. In addition, at all points of contact, the connection between the sheets and the core is assumed to be perfect. Perfect bonding means that the degrees of freedom (DOF) of the upper side of the middle layer are equal to the DOF of the upper face sheet. It also applies exactly to the lower face sheet and lower side of the middle layer. The geometries of the sandwich beam and the assumed coordinate system for the upper sheet, core, and lower sheet are shown in Figure 2.1. The compound beam is bent with a uniform transverse load per unit length along with the x-axis, which is applied to the upper face sheet.

The sandwich structure is built from two materials. As well, the upper and lower sheets are made of steel [52] and the core is made of rubber [52]. The basic values of the material properties are provided in Table 2.1. Both materials are isotropic and ν is the Poisson ratio of materials.

Table 2.1 Material properties [52].

Material	E (GPa)	ν
Steel	210	0.3
Rubber	10^{-2}	0.49

As shown in Figure 2.1, the dimensions of the sandwich beam are chosen in a way that the ratio of the thickness of the middle layer compared to the thickness of the face sheets is 50 and the length of the face sheets in comparison to the beam length is equal to 1000. The beam's boundary conditions are clamped-free. The sheets and the core have different material properties; hence, Young modulus of the compound beam is y-dependent. In this study, no plastic deformation is examined.

2.2. Equivalent single layer Bernoulli-Euler beam solution

In order to make a comparison, in this section, we presented the simplest possible solution for the formulated problem of bending a three-layered sandwich beam. Based on the classical kinematics of unshearable Bernoulli-Euler beam theory, this solution should be considered as valid only as long as the core is sufficiently stiff, such that the shear deformations are not very pronounced. Accordingly, this solution provided us a reference for performing the subsequent thorough evaluation of the properties of the compound model presented in section 3.

2.2.1. General stress and strain in composite beams

Following the basic principles of the calculation of the strains in beams consisting of one material, we determine the strains in composite beams using conventional kinematic assumptions of the Bernoulli-Euler beam theory. Accordingly, this rule is always applied to pure bending and it does not depend on the nature of the beam material. Hence, in a composite beam, the amount of longitudinal strain ε_x linearly changes by moving from the top of the beam to its bottom. The relationship of this strain is as follows:

$$\varepsilon_x = -\frac{y}{\rho} = -\kappa y, \tag{2.1}$$

where y is the distance from the point under study to the neutral axis, ρ is the radius of curvature of the deformed axis of the beam, and κ is the curvature.

To calculate the stress and strain in any type of composite beam, we start from the above-mentioned Eq. (2.1). To illustrate how this operation is performed, we must consider the composite beam shown in Figure 2.3. Correspondingly, this beam is composed of two different materials (materials 1 and 2).

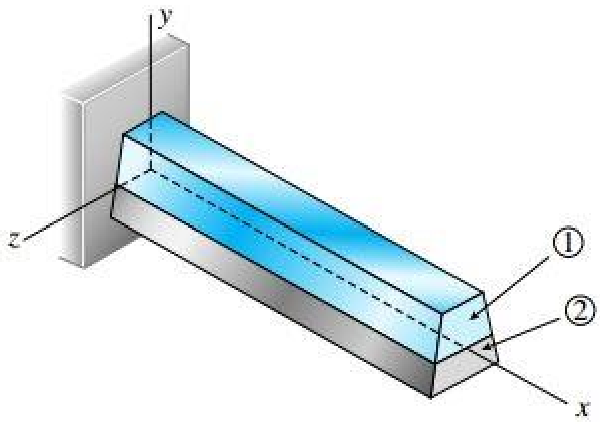

Figure 2.3. Composite beam consists of two materials [54].

The combination of these two materials that makes up a composite beam (as shown in Figure 2.3), such that its behavior against the applied loads can be considered as the behavior of a single material. The overall deformation of this composite beam can be assumed as a single structure. In Figure 2.3, the $x-y$ plane is considered as the symmetry plane and the $x-z$ plane is the neutral plane of the beam. The Euler beam equation arises from a combination of the following four distinct subsets of beam theory: the kinematic, constitutive, force resultant, and equilibrium definition equations. In the following, kinematic and constitutive ones are represented in detail.

2.2.2. Kinematics

The displacement fields in the direction of the x and y axes, shown by $\mathrm{u}(x,y)$ and $\mathrm{w}(x,y)$, respectively, are as follows:

$$u(x,y) = y\frac{d\overline{w}}{dx}, \tag{2.2}$$

$$w(x,y) = \overline{w}(x), \tag{2.3}$$

where $\overline{w}$ is the lateral displacement of the neutral fiber of the beam, the displacement in z-direction is negligible, x is the longitudinal coordinate, and y is the coordinate in the direction of the thickness measured from the neutral fiber of the beam.

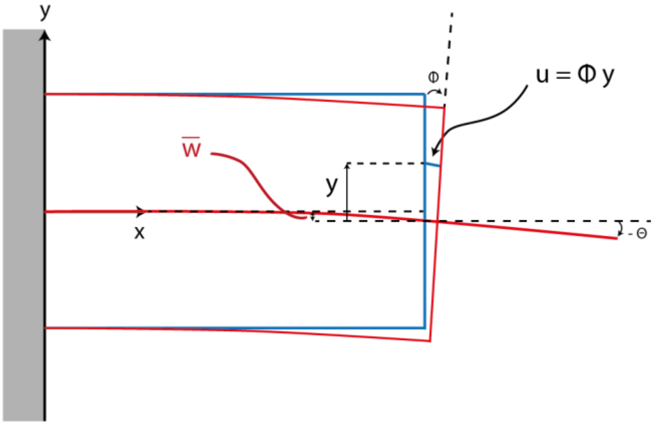

Figure 2.4. Two states of a Euler-Bernoulli beam.

As shown in Figure 2.4, in-plane displacement is accompanied with a rotation of the beam's neutral axis, defined as θ, and by a rotation of the beam's cross-section, defined as ϕ.

$\mathrm{u}(x,y)$ is the displacement in the x-direction across a beam cross section, from which we find the normal strain $\varepsilon_x(x,y)$ by the following equation:

$$\varepsilon_x = \frac{\partial u}{\partial x}, \tag{2.4}$$

For this purpose, it is required to make a few assumptions on how a beam cross section rotates. For the Bernoulli-Euler beam, the assumptions are given by Kirchoff, which dictated how the normals behave [26][53]:

1. Before deformation, straight lines were perpendicular to the midsurfaces, and after deformation, they still remain straight
2. The transverse normals experience no elongation.
3. The rotation of transverse normals is performed in a way that they still remain perpendicular to the beam's axis

With the straight and unstretched normals, we can safely assume that there is a negligible strain in the z direction. With the straight and unstretched normals, we can safely assume that there is a negligible strain in the z direction. Along with normals remaining normal to the neutral plane, we can make the y dependency explicated via a simple geometric expression as follows:

$$u(x, y) = y\phi(x), \tag{2.5}$$

$$\varepsilon_x(x, y) = y\frac{d\phi}{dx}, \tag{2.6}$$

Finally, with normals that are always remaining perpendicular to the cross-sections, we can tie the cross-section rotation ϕ to the neutral plane rotation θ, and eventually to the beam's displacement $\overline{w}$ as:

$$\phi = -\theta = -\frac{d\overline{w}}{dx}. \tag{2.7}$$

2.2.3. Constitutive equation

The constitutive equation describes how both the normal stress σ and normal strain ε within the beam are related to each other. If we were to cut the beam at a given location, we would find a distribution of stresses acting on the beam cross section as shown in Figure 2.5.

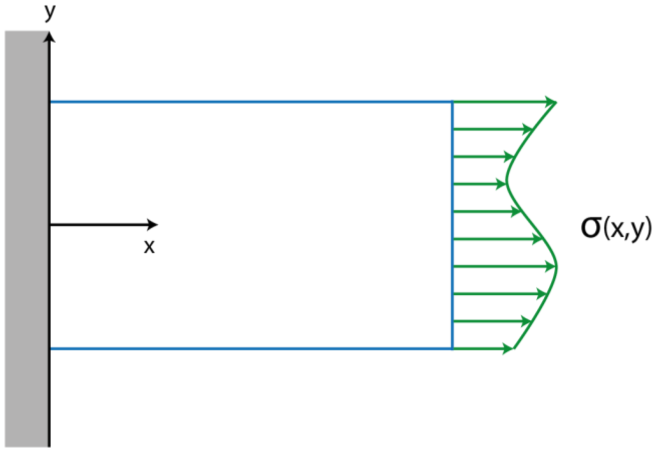

Figure 2.5. Normal stress.

Beam theory typically uses the simple 1-dimensional Hooke's equation,

$$\sigma_x(x,y) = E\varepsilon_x(x,y)\,. \tag{2.8}$$

Of note, the stress and strain are known as the functions of the entire beam cross section (i.e., they can vary with y).

2.2.4. Effective elastic properties

This subsection represents an overview of the properties of the material. In fact, this is a simplification of the whole model. A simple Eulerian beam works with a singular effective bending stiffness. Thereafter, the model is analytically solvable. The sheets and the core have different material properties; hence, Young's modulus of the beam is y-dependent.

The total potential energy (Π) of the beam is constructed from the following two parts: the strain energy (U) and the external force work (W)

$$\Pi = U + W. \tag{2.9}$$

The strain energy can also be assumed from:

$$U = \frac{1}{2}\int_0^l \frac{M^2(x)}{KJ_z}dx\,, \tag{2.10}$$

where l is the length of the beam, respectively (Figure 2.1). Additionally, the bending moment can be written in the following form:

$$M_z = -\int_A \sigma y dA. \tag{2.11}$$

Since this equation is independent of z direction and h, it can be written in the following form:

$$h = 2H_s + H_m, \tag{2.12}$$

where H_s and H_m are explained from Figure 2.2. The total bending moment follows to

$$M_z = b\int_{-\frac{h}{2}}^{\frac{h}{2}} E(y)\kappa y^2 dy, \tag{2.13}$$

κ is the curvature factor and b is width of the sandwich beam model (Figure 2.1). Effective bending stiffness K is now defined as follows:

$$K = b\int_{-\frac{h}{2}}^{\frac{h}{2}} E(y)y^2 dy = b\left(\int_{-\left(\frac{H_m}{2}+H_s\right)}^{-\frac{H_m}{2}} E_{Steel}y^2 dy + \int_{-\frac{H_m}{2}}^{\frac{H_m}{2}} E_{Rubber}dy + \int_{\frac{H_m}{2}}^{\frac{H_m}{2}+H_s} E_{Steel}y^2 dy\right), \tag{2.14}$$

Using beam theory, the deformations induced as a result of the applied distributed load can be determined without solving the two-dimensional equations of the theory of elasticity. The following summary shows the procedure when the cross-section, the modulus of elasticity and the distribution of the bending moment are held constant over the length of the beam:

$$KJ_z\frac{d^2\overline{w}}{dx^2} = M, \tag{2.15}$$

$$KJ_z\frac{d\overline{w}}{dx} = \int M dx + C_1, \tag{2.16}$$

$$KJ_z\overline{w} = \iint M dx\, xC_1 + C_2. \tag{2.17}$$

The two integration constants are represented by C_1 and C_2. These coefficients are determined by applying two boundary conditions and are equal to 0:

$$\overline{w}'_{x=0} = 0 \text{ and } \overline{w}_{x=0} = 0, \tag{2.18}$$

which results in the complete form of the deflection equation.

$$\overline{w}(x) = \frac{f}{24K}(6l^2x^2 - 4lx^3 + x^4), \tag{2.19}$$

In our case, f is a distributed load that is applied on top of the upper face sheet (Figure 2.1). Subsequently, one can determine the displacement at the end point l as follows:

$$\overline{w}(x = l) = \frac{fl^4}{8K}, \tag{2.20}$$

and the respective strain energy is:

$$U = \frac{bl^5f^2}{40K}. \tag{2.21}$$

Chapter 3

Compound beam model

In this chapter, we examine the mathematical modeling of the core as a function of the upper and lower face sheets. This study is performed based on the previous definition of the displacement parameters mentioned in Chapter 2 for the description of the bending of beams.

The sandwich beam is made of three layers. The top and bottom layers are made of steel and the middle layer is made of rubber. The stiffness properties of such a beam are obtained from the properties of the constituent layers by procedures derived in this chapter. Figure 3.1 gives us a brief overview of the geometry of this mathematical model in two dimensions.

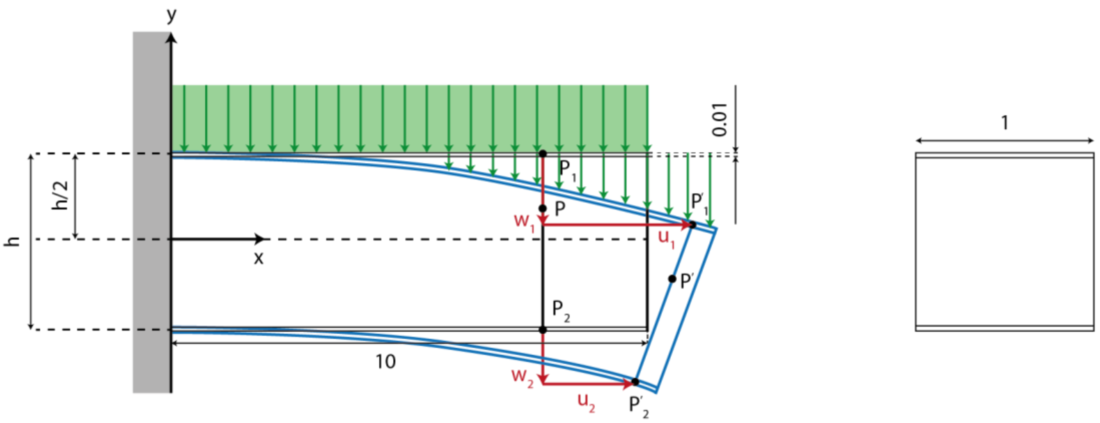

Figure 3.1. Compound beam model under the distributed load.

3.1. Hypotheses

- The beam has a midplane symmetry.
- The layers are isotropic, and the layer axes coincide with the x, y, z axes of the beam.
- The ε_{xz} strain is negligible.
- Under plane stress condition $\sigma_{zx} = \sigma_{xz} = \sigma_{zy} = \sigma_z = 0$, the Hooke's law is as follows:

$$\begin{bmatrix} \varepsilon_x \\ \varepsilon_y \\ \gamma_{xy} \end{bmatrix} = \begin{bmatrix} \frac{1}{E} & -\frac{\nu}{E} & 0 \\ -\frac{\nu}{E} & \frac{1}{E} & 0 \\ 0 & 0 & \frac{1}{G} \end{bmatrix} \begin{bmatrix} \sigma_x \\ \sigma_y \\ \tau_{xy} \end{bmatrix}, \tag{3.1}$$

or in an inverse form:

$$\begin{bmatrix} \sigma_x \\ \sigma_y \\ \tau_{xy} \end{bmatrix} = \begin{bmatrix} \frac{E}{1-\nu^2} & \frac{\nu E}{1-\nu^2} & 0 \\ \frac{\nu E}{1-\nu^2} & \frac{E}{1-\nu^2} & 0 \\ 0 & 0 & G \end{bmatrix} \begin{bmatrix} \varepsilon_x \\ \varepsilon_y \\ \gamma_{xy} \end{bmatrix}. \tag{3.2}$$

In a typical sandwich beam structure, the distortion of the beam section due to transverse shear is illustrated below.

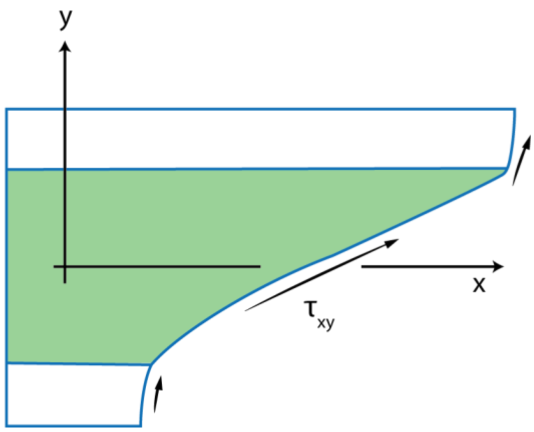

Figure 3.2. Schematic of the Distortion of the Beam Section due to Transverse Shear τ_{xy}

3.2. Kinematics of deformation of the core layer

By assuming that both the upper and lower sheets are simple Bernoulli-Euler beams, the displacement of the middle axis of the core is assumed as an average displacement of the neutral axes of the two sheets as follows:

$$\boldsymbol{u}_M = \frac{1}{2} \begin{bmatrix} u_1(x) + u_2(x) \\ w_1(x) + w_2(x) \end{bmatrix}, \tag{3.3}$$

where the displacements of the upper and lower sheets in x-direction and y-direction are indicated by u_1, u_2 and w_1, w_2 at points P_1 and P_2, respectively, see Figure 3.3. The external force is assumed as the distributed load applied on the upper sheet as shown in Figure 3.1.Thereafter, by deforming the upper sheet, to transfer the displacements to the bottom sheet, a certain deformation appears in the thickness of the core because of its high thickness to length ratio. In this regard, to calculate the deformation in the core, two particles on both upper and lower sheets, namely P_1 and P_2, are chosen as shown in Figure 3.1. After the deformation, these particles move to positions $P_1{}'$ and P_2'.

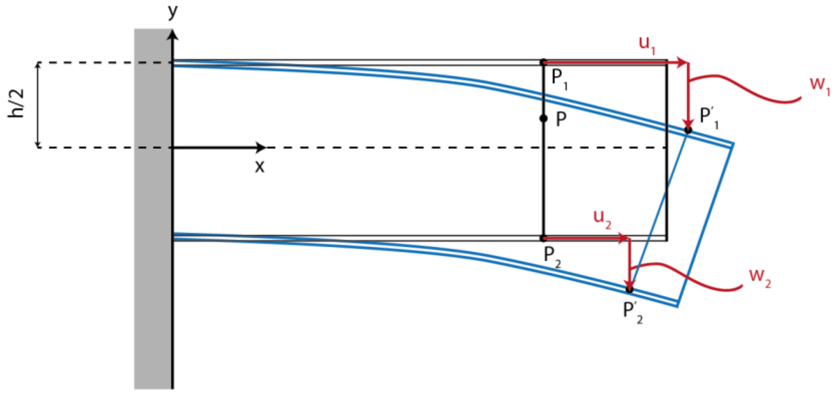

Figure 3.3. Compound beam model dimensions.

we need an approximation of the displacement field in the core layer. The idea is a linear approximation. This approach must satisfy continuity conditions and the displacement field is assumed to vary linearly in the thickness direction. These conditions uniquely determine the displacement field within the body of the core:

$$\boldsymbol{u}_P(x,y) = \begin{bmatrix} \dfrac{u_1(x)+u_2(x)}{2} \\ \dfrac{w_1(x)+w_2(x)}{2} \end{bmatrix} + \begin{bmatrix} \dfrac{u_1(x)-u_2(x)}{h} \\ \dfrac{w_1(x)-w_2(x)}{h} \end{bmatrix} y. \tag{3.4}$$

The displacements of the core are approximated based on the displacements of the two face sheets. Furthermore, the displacements of the core must be linear so as to be consistent with the displacements of the two face sheets at the boundary. To investigate the validity of this approximation and its capability in assuming the correct displacements, the strains at the boundary and throughout the thickness of the core are presented as follows

$$\boldsymbol{\varepsilon} = \begin{bmatrix} \varepsilon_x \\ \varepsilon_y \\ \gamma_{xy} \end{bmatrix} = \begin{bmatrix} \frac{\partial u(x)}{\partial x} \\ \frac{\partial w(x)}{\partial y} \\ \frac{\partial w(x)}{\partial x} + \frac{\partial u(x)}{\partial y} \end{bmatrix}. \tag{3.5}$$

In order to validate the derived mode, we consider several specific cases of deformation and audit the boundary conditions in respect to strain distribution within the core. By substituting Eq. (3.4) into Eq. (3.5), the strain tensor in the core is determined as

$$\boldsymbol{\varepsilon} = \begin{bmatrix} 0 \\ \frac{1}{h}(w_1(x) - w_2(x)) \\ \frac{1}{h}(u_1(x) - u_2(x)) \end{bmatrix}. \tag{3.6}$$

Firstly, we assume $w_1(x) = w_2(x) = u_2(x) = 0$ and the x-direction displacement of the upper sheet as $u_1(x) = kx$, from Eq. (3.5) we obtain the displacement of the core as

$$\boldsymbol{\varepsilon} = \begin{bmatrix} \frac{k}{2} + \frac{k}{h}y \\ 0 \\ \frac{k}{h}x \end{bmatrix}, \tag{3.7}$$

It can be observed that the axial strain of the core is equal to $\frac{k}{2} + \frac{k}{h}y$, strain at the upper boundary in $y = \frac{h}{2}$, is equal to k. The amount of the strain under assumed conditions is the same as the axial strain of the upper face sheet. Also, at the bottom boundary, it is apparent that the axial strain in the core is zero, which is consistent with zero displacement of the bottom face sheet. To further validate the approximation, the following examinations are conducted similar to the above examination of Eq. (3.7).

Vertical displacements of both beams and the horizontal displacement of the upper sheet are considered to be zero ($w_1(x) = w_2(x) = u_1(x) = 0$), and also, the x-direction displacement of the bottom sheet is considered to be $u_2(x) = kx$:

$$\boldsymbol{\varepsilon} = \begin{bmatrix} \frac{k}{2} - \frac{k}{h}y \\ 0 \\ -\frac{k}{h}x \end{bmatrix}. \tag{3.8}$$

Which at the upper and lower boundary confirms the consistency of the displacement field. Also, the elongation of the lower face sheet results in the longitudinal strains linearly distributed over the height of the beam as well as the shear strains, which grows along the axial direction.

At the next stage, the effect of changing the vertical displacement of the upper beam is examined. By assuming $u_1(x) = u_2(x) = w_2(x) = 0$ and substituting $w_1(x) = kx$, in Eq. (3.4) and implementing the results into Eq. (3.5), the following equation is obtained:

$$\boldsymbol{\varepsilon} = \begin{bmatrix} 0 \\ \frac{k}{h}x \\ \left(\frac{k}{2h} + \frac{k}{h}y\right)x \end{bmatrix}. \tag{3.9}$$

Yet again, the strains in the core and at the boundaries are in agreement with the axial and through the thickness strains of the face sheets. Similarly, $w_1(x) = u_2(x) = u(x) = 0$ and $w_2(x) = kx$

$$\boldsymbol{\varepsilon} = \begin{bmatrix} 0 \\ -\frac{k}{h}x \\ \left(\frac{k}{2h} - \frac{k}{h}y\right)x \end{bmatrix}. \tag{3.10}$$

The same conclusion similar to the one achieved in Eq. (3.9) is observed to occur in Eq. (3.10). For the case of inclination of both beams $w_1(x) = w_2(x) = kx$ and vanishing displacements in x we observe a simple shear deformation

$$\boldsymbol{\varepsilon} = \begin{bmatrix} 0 \\ 0 \\ k \end{bmatrix}. \tag{3.11}$$

The trivial longitudinal stretch $u_1(x) = u_2(x) = kx$ results in

$$\boldsymbol{\varepsilon} = \begin{bmatrix} k \\ 0 \\ 0 \end{bmatrix}. \tag{3.12}$$

For a rigid body rotation, displacements are $u_1 = -k\frac{h}{2}$, $u_2 = k\frac{h}{2}$, $w_1(x) = w_2(x) = kx$, and the implementation in Eq. (3.5) indeed results in vanishing strains:

$$\boldsymbol{\varepsilon} = \begin{bmatrix} 0 \\ 0 \\ 0 \end{bmatrix}, \tag{3.13}$$

Eq. (3.13) indicates a whole-body movement as well as a separation from the axial boundary. The approach to compute the strain energy in the middle layer of the compound beam for the given deformations w_1, u_1, w_2, and u_2 of the face sheets is given as follows:

$$U_{Mid.layer} = b\int_0^L \int_{-h/2}^{h/2} (\frac{1}{2}E_{Rubber}(\varepsilon_x^2 + \varepsilon_y^2) + 2\mu\varepsilon_{xy}^2)dydx, \tag{3.14}$$

$$\mu = \frac{E_{Rubber}}{2(1+\nu)}. \tag{3.15}$$

Notably, the strain energy of the middle layer depends on the strains induced in this layer through the displacements of the face sheets. Furthermore, the strain energy of the beams is separated into a part due to tension and a contribution from bending:

$$U_{Beam} = U_{bending} + U_{Tension}, \tag{3.16}$$

$$U_{bending} = \int_0^l \frac{M^2}{2\, E_{steel}\, J_z}\, dx = \frac{1}{2}E_{steel}\, J_z \int_0^l \left(\frac{d^2 w_i}{dx^2}\right)^2 dx, \tag{3.17}$$

$$U_{Tension} = \int_0^l \frac{N^2}{2\, AE_{steel}}\, dx = \frac{1}{2}E_{steel}A \int_0^l \left(\frac{du}{dx}\right)^2 dx, \tag{3.18}$$

$$J_z = \frac{1}{12}H_s^3 . b, \tag{3.19}$$

$$A = H_s\, .\, b. \tag{3.20}$$

The total strain energy of the sandwich structure is determined using the following equation:

$$U^{total} = U_{Mid.layer} + U_{Beam,up} + U_{Beam,down}. \tag{3.21}$$

The strain energies of the face sheets are different based on their displacements and locations. The strain energies of both beams are similar and $U_{Beam,up}$ represents the amount of bending and tension energy in upper face sheet and $U_{Beam,down}$ represents the energies for lower face sheet.

Chapter 4

Approaches to analyzing the compound beam model

Herein, we present some methods for finding the state of static equilibrium by minimizing the total potential energy of the compound model of the sandwich beam. To fulfill this, the field variables of $w_1(x)$, $u_1(x)$, $w_2(x)$, $u_2(x)$ need to be approximated, such that we represent them by a finite set of variables. Thereafter, two approaches are considered: global Ritz approximation and finite element approximation, which needs a C1-continuous approximation to fulfill the kinematic requirements of the beam theory.

4.1. Variational principles

Variation calculus seeks to find a set of paths and curves with longitudinal extremums as both continuous and derivative functions (often referred to as the minimum or maximum in physical problems). In mathematics, the value of this extremum is denoted by the following definite integral:

$$R = \int f(t, y, \dot{y}) dt. \tag{4.1}$$

Functionals are often expressed as the definite integrals in which their functions and derivatives appear. Moreover, the functions that maximize and minimize the functionals are found in the calculus of variations using the Euler-Lagrange equations.

To derive the functionals and the overall Euler-Lagrange equations, three variational principles are used as follows:

a) The Principle of Conservation of Energy
b) The Principle of Virtual Work
c) The Principle of Minimum Potential Energy

The minimization is done after performing the displacement approximations with the help of the two methods that are explained in the following sections.

4.2. Ritz method implementation

To approximate the displacements in the upper and lower face sheets, the Ritz method is utilized. The Ritz method is a numerical method which is based on variational principles. Accordingly, the principle of minimum potential energy is the main principle behind the energy method developed by Ritz. Using this method, the approximation is done by assuming the displacements as a power series:

$$q = \begin{bmatrix} q_{1,1}^{u}, q_{1,2}^{u}, q_{1,3}^{u}, \dots, q_{1,n}^{u} \\ q_{1,2}^{w}, q_{1,3}^{w}, q_{1,4}^{w}, \dots, q_{1,n}^{w} \end{bmatrix}, \tag{4.2}$$

$$u_i(x) = \sum_{k=1}^{n} q_{i,k}^{u} x^k \qquad i = 1,2, \tag{4.3}$$

$$w_i(x) = \sum_{k=2}^{n} q_{i,k}^{w} x^k \qquad i = 1,2, \tag{4.4}$$

where the vector of degrees of freedom q comprises the coefficients in the approximations of the variables to be determined. To simplify these equations, some of the coefficients are assumed to be zero as shown in Eq. (4.2). The boundary conditions at $x = 0$ require the displacements at that point to be zero, hence the coefficients of those points will vanish from the series solution.

By substituting Eqs. (4.3) and (4.4) into Eq. (3.4), the displacement of an arbitrary point in the core (point P in section 3.2) is found. Additionally, the strain of the core is determined by substituting the displacement components, which are derived in Eqs. (4.3) and (4.4) in Eq. (3.5).

Finally, the strain energy of the beam is determined as a quadratic form with a stiffness matrix K:

$$U^{total} = \frac{1}{2} q^T K q. \tag{4.5}$$

To determine the stiffness matrix of the beam, the total energy of the beam is considered as a function of the coefficients of the Ritz approximation as

$$K = \frac{\partial^2 U}{\partial q^2}. \tag{4.6}$$

In addition, the linear form of the potential of external force using the vector of generalized forces is defined as:

$$W^{total} = -b\int_0^l f\, w_i dy = -q^T F, \tag{4.7}$$

where f is the distributed load. Thereafter, similar to the stiffness matrix, the resultant matrix in the vectorized form is derived:

$$F = -\frac{\partial W}{\partial q}. \tag{4.8}$$

The equations of static equilibrium follow from the principle of minimality of the total energy $U^{total} + W^{total}$. We seek the minimum by demanding that the derivatives with respect to the degrees of freedom q must vanish. Eventually these results into the following linear algebraic system of equations:

$$F = Kq. \tag{4.9}$$

The Ritz's coefficients are then computed from Eq. (4.9) and the expressions for the approximated displacement of the upper and the lower face sheets are determined.

4.3. Finite Element Method implementation

As an alternative to the global polynomial approximation in the form of Eqs. (4.3) and (4.4), we consider a finite element scheme, which is a subclass of the Ritz method with localized shape functions. One can thus consider two finite elements on top of each other as a compound problem specific finite element, consisting of the finite elements of both beams and a piece of the middle layer between them within the finite element. Similar to the previous section, the displacement of the core is calculated through the two displacements of the surrounding sheets. In the standard Finite Element Method with nodal identity shape functions, the continuity of the derivative of displacement between elements is not guaranteed. However, assuming derivatives of deflection as the additional DOF, the continuity of the derivative of deflection is also guaranteed. This prevents the kink production in the nodes, which is not allowed in the kinematics of Bernoulli-Euler beams. Cubic shape functions [52] are used to approximate the deformation of sandwich beam within an element. These functions are shown in Figure 4.1. To further simplify the integrals for calculation of the total strain energy, the shape functions and the displacement approximations are transformed into the local coordinates. In local coordinate system, each of the shape functions has either the value 1 or the derivative 1 in one of the two nodes of the element, whereas all other nodal values and derivatives vanish. The mapping relation between global coordinate and local coordinate ζ is demonstrated in Eq (4.10). We discretized the length of the beam into n elements, numbered from 1 to n. An element number i has nodes with numbers i-1 at the left and i at the right. At each element a local coordinate ζ is introduced, which varies from -1 to 1.

$$\zeta(x) = \frac{2x - (x_{i-1} + x_i)}{x_i - x_{i-1}}, \tag{4.10}$$

Cubic shape functions are defined as follow:

$$S_1 = \frac{1}{4}(2 - 3\zeta + \zeta^3), \tag{4.11}$$

$$S_2 = \frac{1}{4}(-1 + \zeta)^2(1 + \zeta), \tag{4.12}$$

$$S_3 = \frac{1}{4}(2 + 3\zeta - \zeta^3), \tag{4.13}$$

$$S_4 = \frac{1}{4}(-1 + \zeta)(1 + \zeta)^2. \tag{4.14}$$

Utilizing these shape functions, the displacement of the i-th element of j-th face sheet is evaluated as given by Eqs. (4.15) -(4.16) subject to continuity conditions of Eqs. (4.17) -(4.18)

$$u_j^{(i)} = u_{i-1,j} \,.S_1 + \epsilon_{i-1,j}.S_2 + u_{i,j}.S_3 + \epsilon_{i,j}.S_4, \tag{4.15}$$

$$w_j^{(i)} = w_{i-1,j} \,.S_1 + \theta_{i-1,j}.S_2 + w_{i,j}.S_3 + \theta_{i,j}.S_4, \tag{4.16}$$

$$u_j^{(i)}(-1) = u_{i-1,j}, \qquad u_j^{(i)}(1) = w_i, \qquad \partial\zeta u_j^{(i)}(-1) = \epsilon_{i-1}, \qquad \partial\zeta w_j^{(i)}(1) = \epsilon_i, \tag{4.17}$$

$$w_j^{(i)}(-1) = w_{i-1,j}, \qquad w_j^{(i)}(1) = w_i, \qquad \partial\zeta w_j^{(i)}(-1) = \theta_{i-1},$$
$$\partial\zeta w_j^{(i)}(1) = \theta_i, \tag{4.18}$$

in which, θ and ϵ are the first derivative of w and u with respect to local coordinate ζ, respectively. The following nodal variables play thus the role of the degrees of freedom of the finite element model: u , w, θ, ϵ

The discretized form of Eq (3.4) can be recast into the following equations:

$$u = \frac{1}{2}(u_1^{(i)}+u_2^{(i)})+\frac{1}{h}(u_1^{(i)}- u_2^{(i)})\text{y}, \tag{4.19}$$

$$w = \frac{1}{2}(w_1^{(i)}+w_2^{(i)})+\frac{1}{h}(w_1^{(i)}- w_2^{(i)})\text{y}, \tag{4.20}$$

Similar to the Ritz method, the displacements are approximated through the elements. Length of each element is assumed as follows:

$$l_0 = x_i - x_{i-1}. \tag{4.21}$$

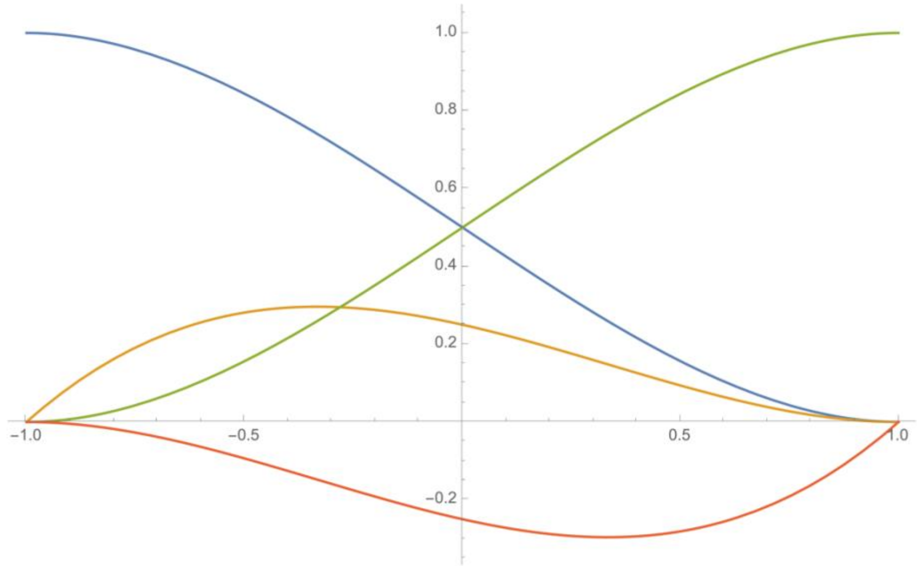

Figure 4.1. Polynomial shape functions.

The bending and tension energy of i-th element is calculated with the help of Eq. (4.22) -(4.23)

$$U_{w_j^{(i)}} = \frac{1}{2} E_{steel}\, J_z \int_{-1}^{1} w''\, dx = \frac{1}{2} E_{steel}\, J_z \int_{-1}^{1} \left(\partial_\zeta^2 w (\partial_x \zeta)^2\right)^2 \partial_\zeta x\, d\zeta, \tag{4.22}$$

$$U_{u_j^{(i)}} = \frac{1}{2} E_{steel}\, A \int_{-1}^{1} u'\, dx = \frac{1}{2} E_{steel}\, A \int_{-1}^{1} \left(\partial_\zeta u (\partial_x \zeta)\right)^2 \partial_\zeta x\, d\zeta, \tag{4.23}$$

In order to transfer the derivatives w' and u' from global coordinates to the local coordinates, $\partial_\zeta x$=$l_0/2$ and $\partial_x \zeta = 2/l_0$ is derived which results into Eqs. (4.24) -(4.25).

$$U_{w_j^{(i)}} = \frac{1}{2} E_{steel}\, J_z (\frac{2}{l_0})^3 \int_{-1}^{1} \left(\frac{\partial^2 w_i}{\partial x^2}\right)^2 d\zeta, \tag{4.24}$$

$$U_{u_j^{(i)}} = \frac{1}{2} E_{steel} A (\frac{2}{l_0})^1 \int_{-1}^{1} \left(\frac{\partial u_i}{\partial x}\right)^2 d\zeta. \tag{4.25}$$

Total bending and tension energies of both face sheets are calculated from Eq. (4.26) -(4.27)

$$U_{Bending} = \sum_{i=1}^{n} \sum_{j=1}^{2} U_{w_j^{(i)}}, \tag{4.26}$$

$$U_{Tension} = \sum_{i=1}^{n}\sum_{j=1}^{2} U_{u_j^{(i)}}. \tag{4.27}$$

To determine the total strain energy of the whole beam, the strain energy of the middle layer is also needed. For this purpose, the strain tensor is expressed in the following form utilizing the local coordinate ζ:

$$\boldsymbol{\varepsilon} = \begin{bmatrix} \frac{2}{l_0}\frac{\partial u}{\partial \zeta} \\ \frac{\partial w}{\partial y} \\ \frac{2}{l_0}\frac{\partial w}{\partial \zeta} + \frac{\partial u}{\partial y} \end{bmatrix}. \tag{4.28}$$

For this purpose, we substituted Eq. (4.28) in Eq. (3.14) and obtained Eq. (4.29) as follow

$$U_{Mid.layer} = b\int_{-1}^{1}\int_{-h/2}^{h/2}(\frac{1}{2}E_{Rubber}(\varepsilon_\zeta^2 + \varepsilon_y^2) + 2\mu\varepsilon_{\zeta y}^2)dyd\zeta, \tag{4.29}$$

By substituting Eqs. (4.26) -(4.27) and (4.29) in Eq (3.21), U^{total} is obtained. Subsequently, the overall differential Euler-Lagrange equation is transformed into a system of linear nonhomogeneous algebraic equations. The structure of the stiffness matrix of the beam is demonstrated in Figure 4.2 and obtained from Eq. (4.6). As clearly can be seen, the degrees of freedom in nodes, which are separated by more than 1 element, are uncoupled.

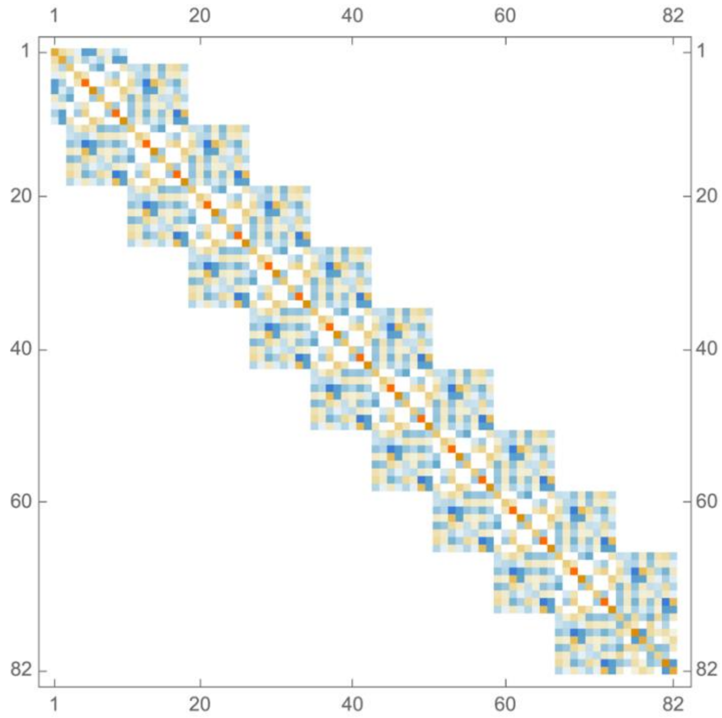

Figure 4.2. The profile structure of the stiffness matrix.

Same as in section 4.2, unknown coefficients q are obtained by solving the linear system of equations in Eq. (4.9).

4.4. ABAQUS simulations

At this stage, the commercial finite element simulation program ABAQUS is employed as a validation technique, since it displays valid results within the broad range of parameter values. Using ABAQUS, the cantilever beam is simulated. In doing so, we partition the beam into three sections in order to take the three layers of the sandwich beam into account. A two-dimensional quadratic element (CPS8) is then chosen.

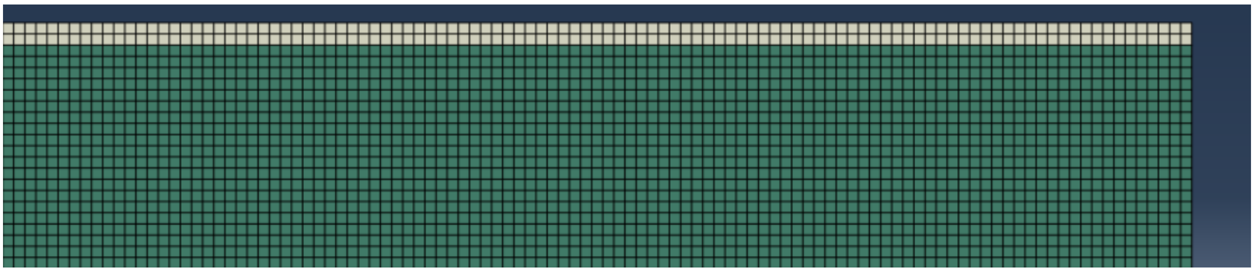

Figure 4.3.The meshing of the cantilever beam at a corner.

Afterward, the beam is meshed into 163879 elements as shown in Figure 4.3. Notably, all element sizes are set at 0.005 m. Although the size of the mesh does not play a critical role in the overall simulations, the elements are still chosen to be very small in leu of the simplicity of the model to achieve higher accuracy.

The material properties of the beam are set to data provided in this study, the upper and lower face sheets are modeled along with the core as a two-dimensional continuum at plane stress conditions. Accordingly, the core resists shear, transverse, and longitudinal loads. In addition, at all points of contact, the connection between the sheets and the core is assumed to be perfect. Perfect connection means that the degrees of freedom (DOF) of the upper side of the middle layer are equal to the DOF of the upper face sheet. It applies exactly to the lower face sheet and lower side of the middle layer also. The geometries of the sandwich beam and the assumed coordinate system for the upper sheet, core, and lower sheet are shown in Figure 2.1. The compound beam is bent with a uniform transverse load per unit length along with the x-axis, which is applied to the upper face sheet.

The sandwich structure is built from two materials. As well, the upper and lower sheets are made of steel [52] and the core is made of rubber [52]. The basic values of the material properties are provided in Table 2.1. Both materials are isotropic and ν is the Poisson ratio of materials. Finally, the beam is connected on its outer leftmost nodal points to an immovable boundary; hence, all the degrees of freedom are constrained there, which corresponds to the clamping boundary condition.

The geometric characteristics of the beam are found in section 2.1. On the upper surface of the beam, a distributed load of 1000 N/m^2 is assumed. Accordingly, all the results are obtained using geometrically linear simulations.

Chapter 5

Results of numerical experiments and validation

In this chapter, the results of the calculations performed based on the numerical schemes discussed in previous chapters, are provided. The beam is subjected to a distributed load in order to be analyzed using different methods. These methods can be categorized into two different mathematical proceedings. Three numerical analysis methods are used in this regard, namely FEM, Ritz methods, and ABAQUS 2D simulation. The analytical models include equivalent single layer beam model. The effect of different parameters variation such as height of the beam, elastic moduli of the constituents, and the number of interpolation functions are also investigated.

5.1. Convergence study

Numerical models initially require a convergence study before being considered as validated. The effect of increasing the number of terms for the Ritz approximation on the calculated total energy of the beam is presented in Figure 5.1. Accordingly, by increasing the number of interpolation order, the convergence is firstly observed for up to 20 terms, and then the results are getting essentially less accurate. Of note, this behavior does not naturally occur in abstract mathematics. However, at increasing number of approximation functions, the stiffness matrix becomes more and more ill-conditioned, the accuracy of solving the linear system of equations diminishes, and errors occur as a result of rounding employed by the commercial program Mathematica. Thus, for the simplified calculations, the number of terms for the following results pertaining to Ritz model is set to 10.

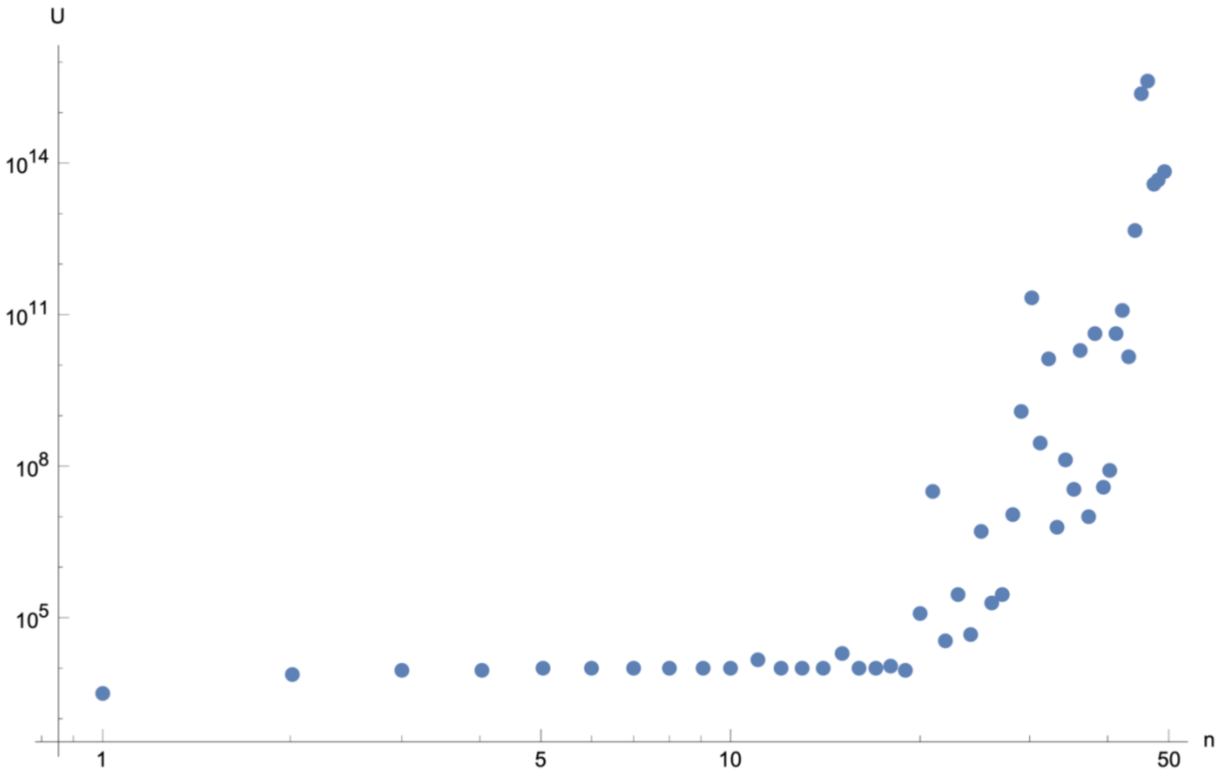

Figure 5.1. Convergence of the Ritz model versus the number of terms employed in approximation

As mentioned earlier, the convergence of numerical methods is of utmost importance. For the following FEM analyses, it is attempted to calculate the total energy convergence by increasing the number of elements. As shown in Figures 5.2-5-4, total energy of the beam is plotted against the number of elements. Additionally, by increasing the elastic modulus of the core, the optimum number of elements for convergence is investigated for conducting further analyses.

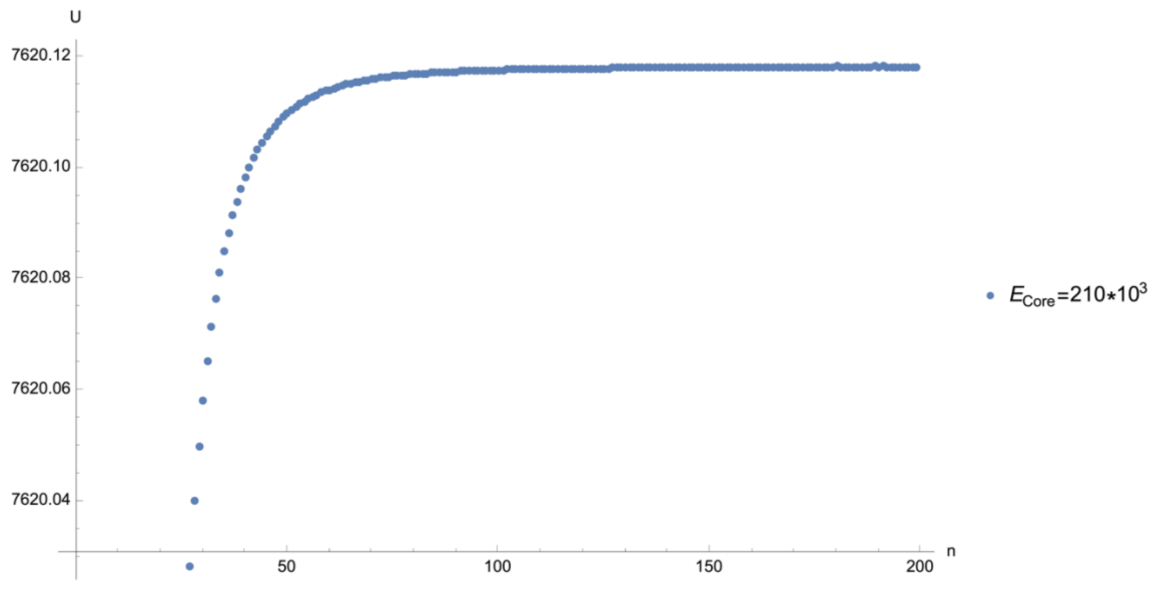

Figure 5.2. Total energy of the beam versus the number of elements for $E_{Core} = 210 \,.\, 10^3$.

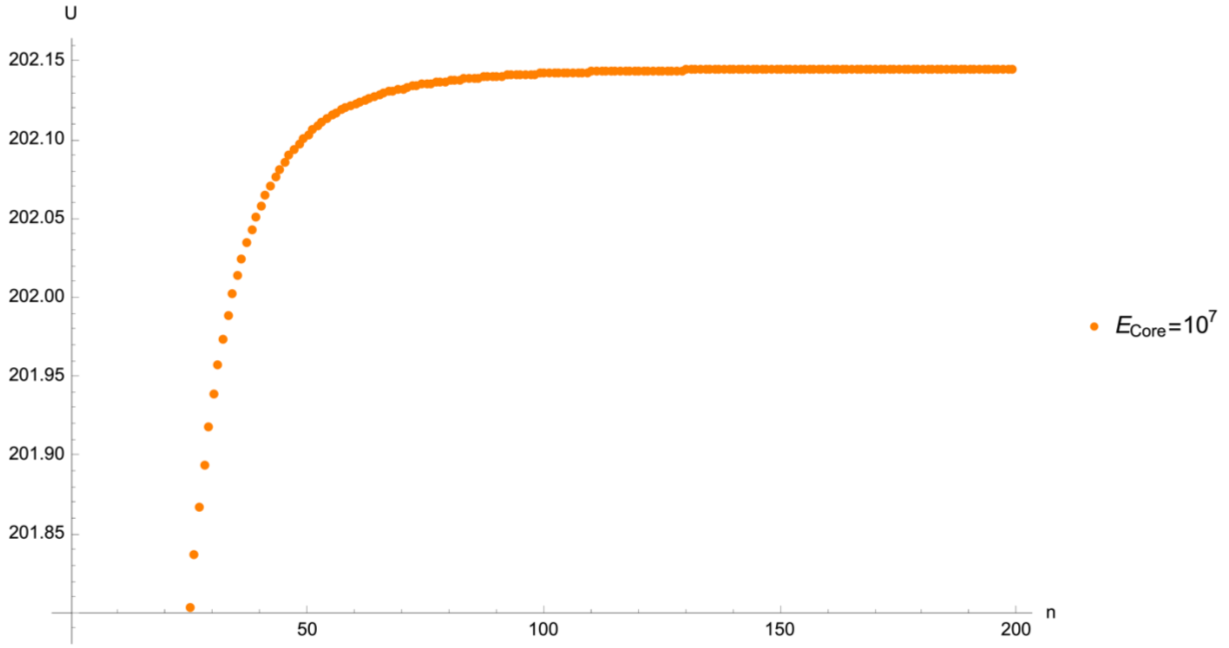

Figure 5.3. Total energy of the beam versus the number of elements for $E_{Core} = 210 \,.\, 10^7$.

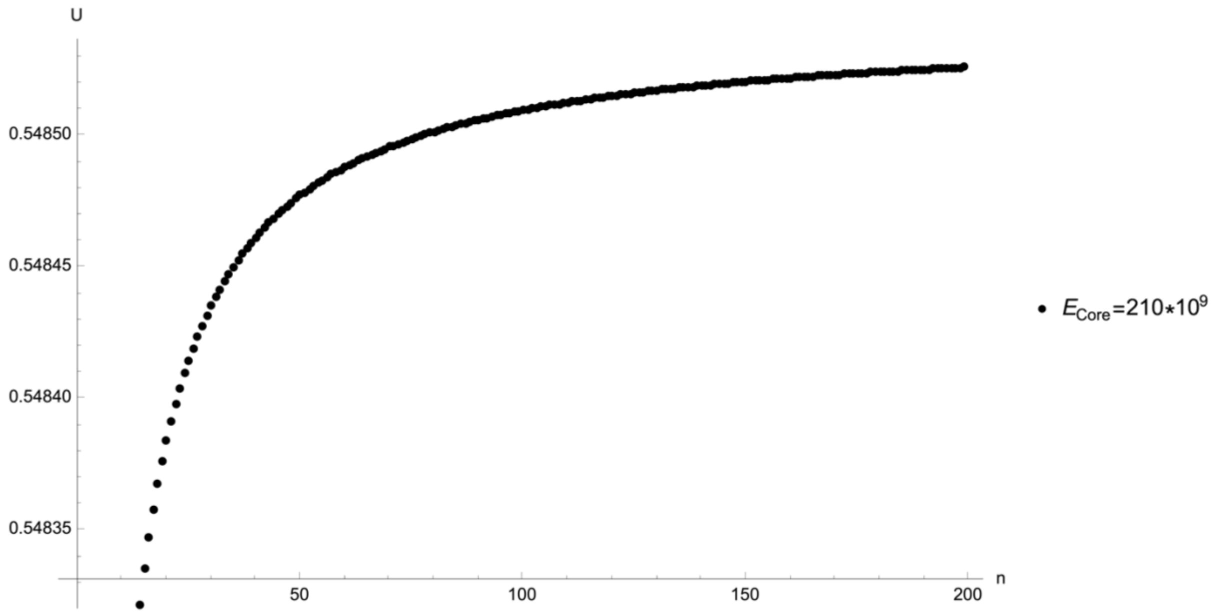

Figure 5.4. Total energy of the beam versus the number of elements for $E_{Core} = 210 \,.\, 10^9$.

In Figures 5-2-5-4, after 68 elements, the total calculated relative increments in the strain energy becomes less than our defined tolerance 10^{-6}. The relative error is calculated as follow

$$Erorr_{Relative} = \frac{U_i - U_{i-1}}{U_{i-1}}. \tag{5.1}$$

This convergence is also observed to occur in all the above figures. The increase in the number of elements plays a much larger part in capturing the essence of the material, since the beam is partially observed to be isotropic. By increasing elements number, in Figures 5-2-5-4 the results are not varied more than 14%.

In the following section, Ritz and FEM models used in the present study will be validated. In addition, by analyzing the results obtained from Figures 5-2-5-4 and Eq. (5.1) the optimum number of elements is assumed to be 68. As shown in this section, the convergence of our model is not strongly affected by different elastic moduli; in all three studies, the magnitude of strain energy converged to a constant value.

5.2. Validation

In chapter 3, a compound beam model was presented. By comparing the results obtained from the compound beam model and 2D ABAQUS simulations, the presented model is validated. The deflection of a beam against the changes in the elastic modulus ratio of the rubber core to the steel face sheets is illustrated in Figure 5.5 As we see, both the simple beam model and the compound beam model predict accurate responses for stiffness ratios under 500. However, as can be seen, the error of the simple beam model is more pronounced with higher ratios. On the other hand, the compound beam model predicts an accurate deflection compared to the reference solution. The manifested difference is presumed as a result of the differences in the effective elastic modulus of the beam. It is found that the simple beam model cannot accurately display the overall deflection of the beam, since after a ratio of 100, the kinematics of the deformation of the Bernoulli-Euler beam theory is insufficient to describe the more complicated behavior of the sandwich structure at such high stiffness ratios. In Figure 5.5, we assumed 10 as the polynomial order of the Ritz method according to the convergence study conducted in the previous section.

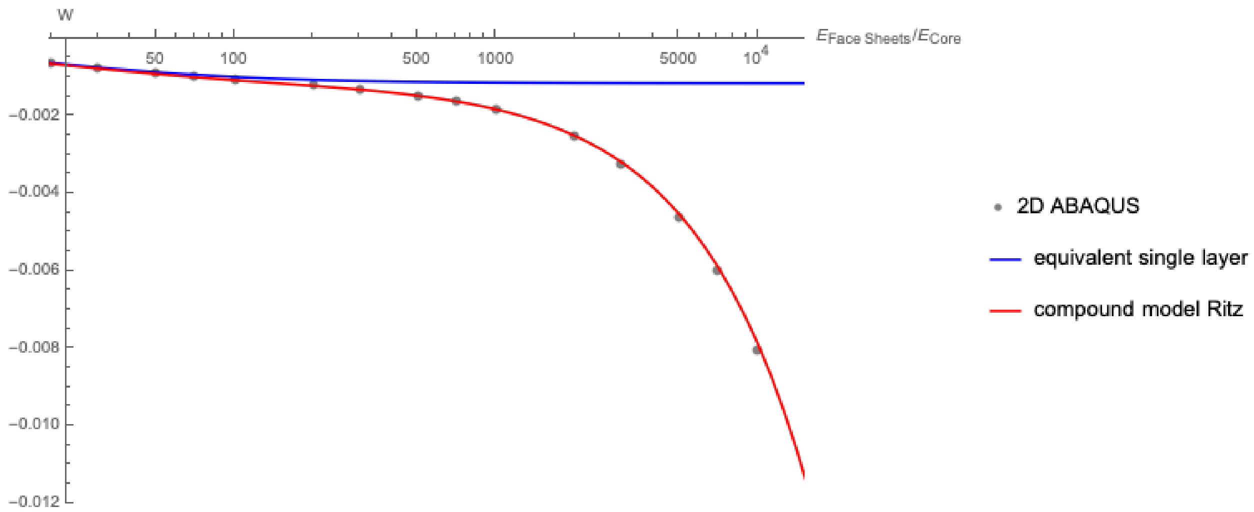

Figure 5.5. Deflection of the beam versus elastic modulus ratio.

In Figure 5.6 we demonstrate the variations of the total strain energy of the beam for varying stiffness ratios at a given loading computed using the above-mentioned 4 methods. It must be noted that the Ritz method and the FE method are in agreement, the difference between the two models is within our defined tolerance range from 10^{-3} to 10^{-6}. Accordingly, the results of the developed compound model are in good agreement with the 2D ABAQUS simulation as a reference solution. As discussed earlier, the changes in the elastic modulus ratio have not been accurately reflected in the equivalent single layer model. In Figure 5.6, the total energy of the beam is observed to reach 10^5 for a beam with nearly no core strength. Correspondingly, this phenomenon can be explained by assuming a massive deflection in the upper face sheet, a nearly flattened state for the core, as well as a small deflection for the bottom face sheet. Figure 5.7 shows a zoomed in version of Figure 5.6, in order to indicate the separation point of the simple beam model with the rest of them.

The graph presented in Figure 5.6 can be explained in 3 sections. As indicated, from point A to point B, all these 4 methods provide the same response, the difference between two results is less than our relative error 10^{-3}. From point B to point C, the three numerical methods again predict the same response, but they start to deviate from the simple beam model since the shear deformation starts growing as the rubber core is restricted by the longitudinal strain of the face sheet. This effect is not captured by the simple model. From point C forward, even the transverse stiffness of the core is getting so small, that the upper face sheet withstands the external loading on its own without the support of the lower one. By ratios above 10^8, the core seemingly ceases to have an interaction with the movements of the top or bottom layer. Further increases in this parameter have no longer influence on the total strain energy of the beam and the graph continues on a horizontal line.

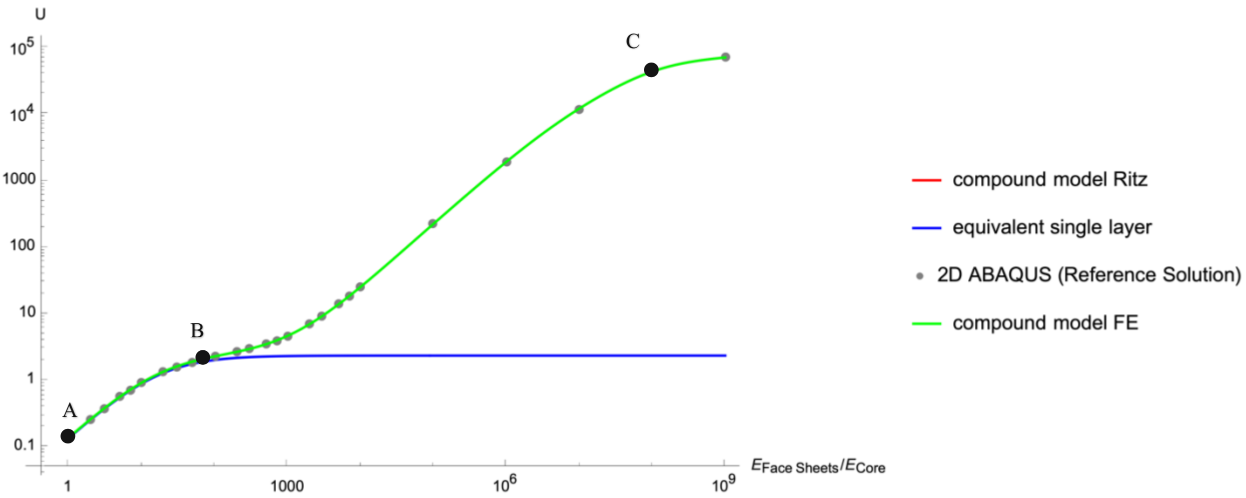

Figure 5.6. Changes in the total strain energy of the beam versus elastic modulus ratio.

To further validate the accuracy of the presented study, a section of the graphs between points B and C in Figure 5.6 is presented in a larger scale. In Figure 5.7, the use of the compound beam model in both FEM and Ritz methods has proven to be in relative agreement with the results obtained with the ABAQUS simulations.

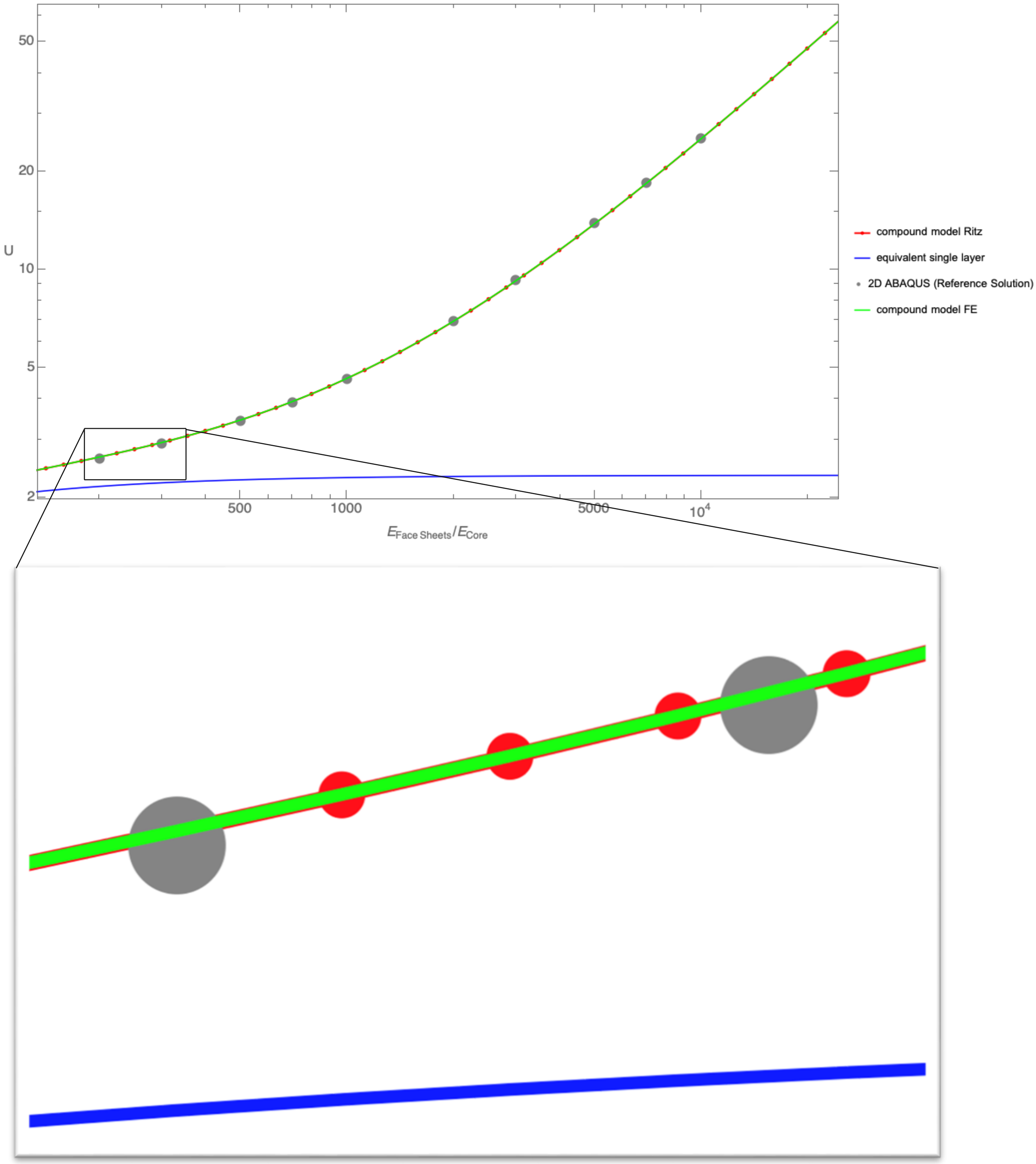

Figure 5.7. Changes in the total strain energy of the beam versus elastic modulus ratio (zoomed).

Similarly, the results presented in Figure 5.8 prove the accuracy of the presented model. The deflection of the mid plane of the beam calculated through the compound beam model is compared with the 2D simulations of ABAQUS. As shown, the model proves to be capable in determining the deflection of the beam with less computational time and resources and acceptable accuracy.

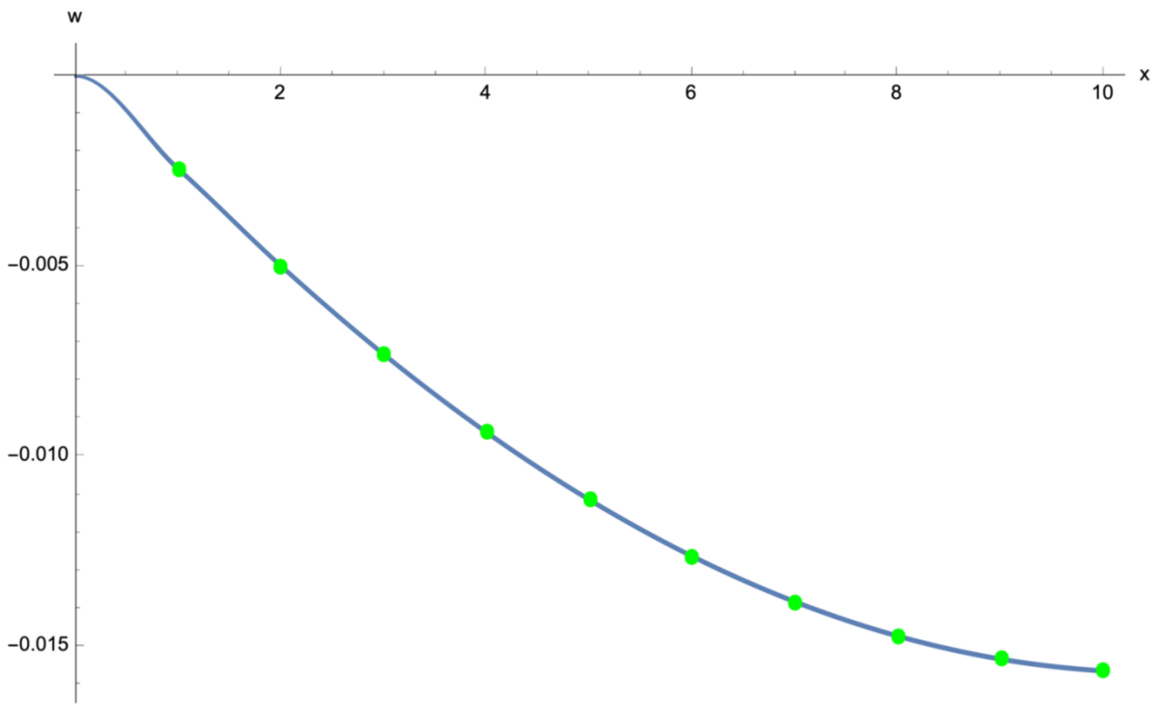

Figure 5.8. Deflection of the top surface of the upper face sheet with 10 elements.

5.3. Parametric study

To investigate the effects of beam thickness on the overall strain energy of the sandwich beams of varying thicknesses and core strengths, all under a constant distributed load, as mentioned in the previous chapters, Ritz method is used for obtaining the results presented in Figure 5.9. By increasing the thickness of the beam, it is observed that the energy changes assume a downward trend until the thickness effects are no longer visible. This phenomenon is related to the deformation transference in the core, and this is more apparent if the core has a lower strength than the face sheets. The peculiar trends observed for the core strengths smaller than 210×10^3 require further investigations.

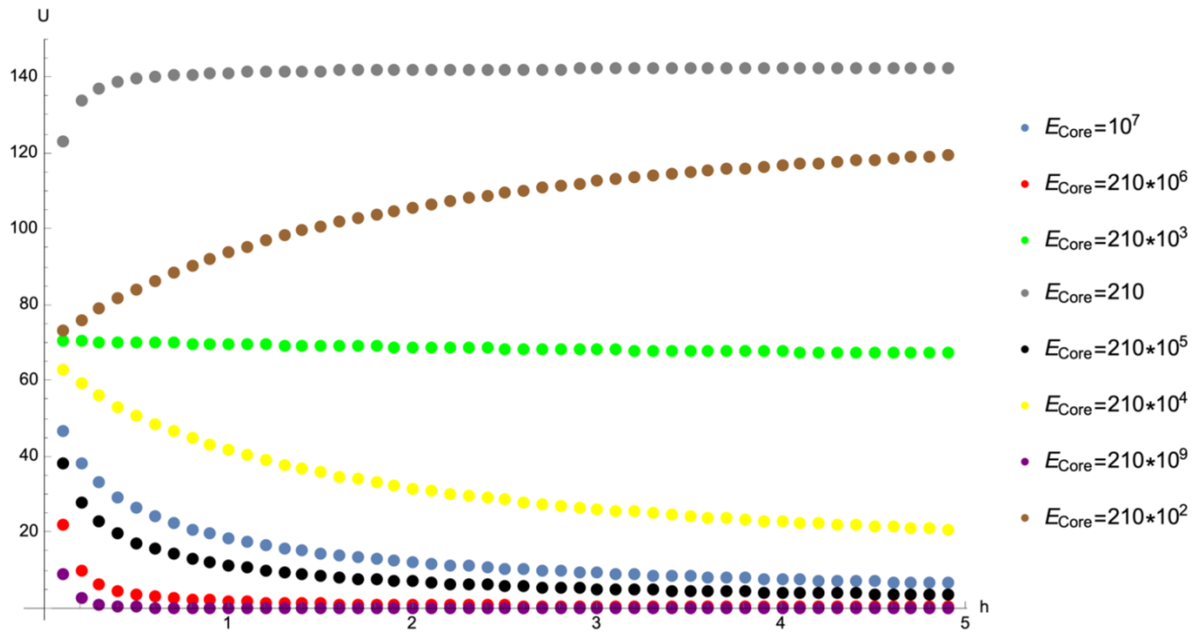

Figure 5.9. Variation of energy versus height of core.

The deformation of the beam is calculated using both the Ritz method and 2D ABAQUS simulations, as shown in Figures 5.10-5.12. Figure 5.10 shows the deflection of a beam with a core ratio of 1, which essentially makes the sandwich beam a whole steel beam. As can be seen in Figure 5.10, the maximum deflection and the structural deformation of the beam according to both Ritz and ABAQUS look similar. From these figures, it can quantitatively be seen that the deformation from the structural mechanics model matches the deformation from the continuum mechanics model. Due to the low strength of the material in the second case, the area of the model with the maximum deflection magnitude is significantly more than the first case. In the third case, in addition to the increased amount of deformation, its behavior also changed. due to the fact that in the 3rd case the material of the core and face sheets are very different, therefore this s shaped relationship appears. In addition, in the representation of diagrams, the same scaling factor is used.

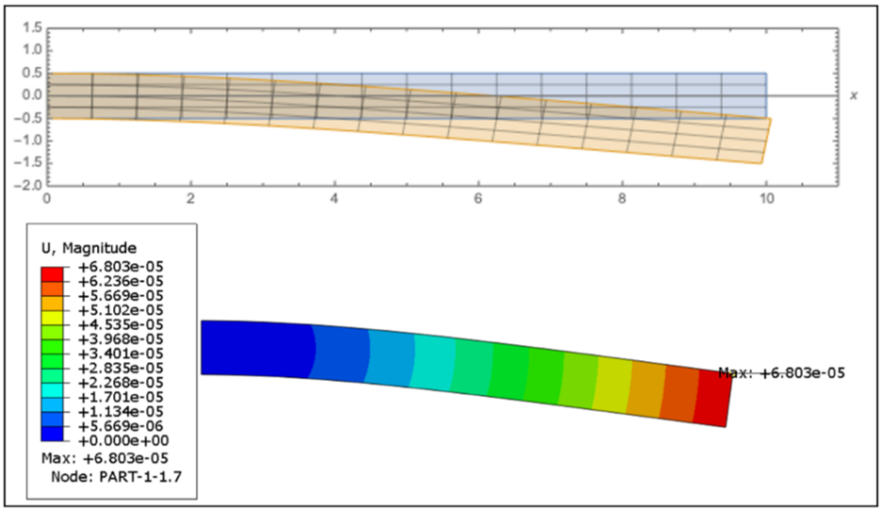

Figure 5.10. Deflection of the beam using Ritz and ABAQUS for $E_{Core} = E_{Face\ Sheets}$.

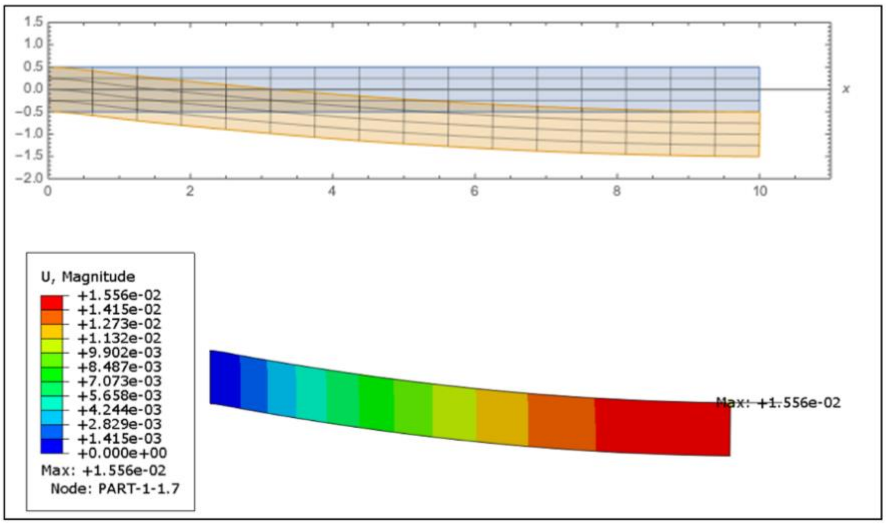

Figure 5.11. Deflection of the beam using Ritz and ABAQUS for $E_{Core} = E_{Face\ Sheets}.10^{-2}$.

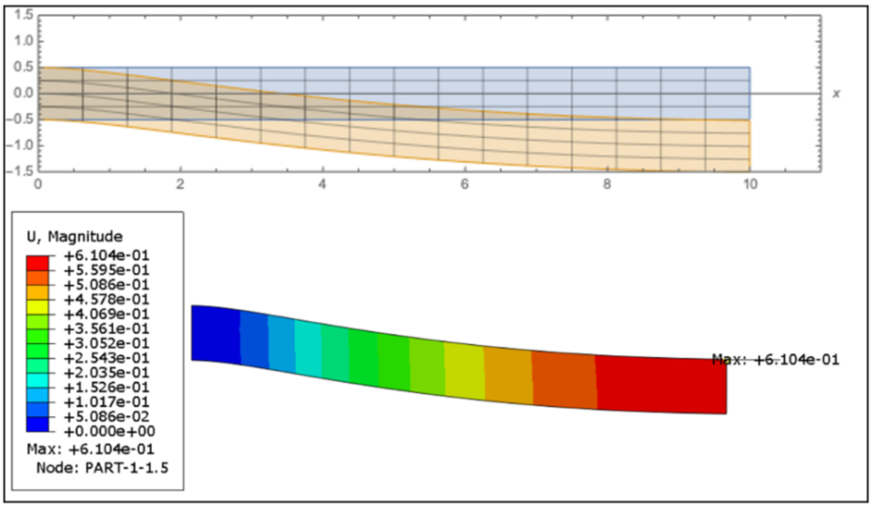

Figure 5.12. Deflection of the beam using Ritz and ABAQUS for $E_{Core} = E_{Face\ Sheets} . 10^{-6}$.

Chapter 6

Conclusion

Two approximation methods, namely simple beam model and compound beam model, are utilized to determine the deflection of a sandwich beam under distributed loading. As it is extensively described in chapter 5 of this study, the simple beam model (equivalent single layer) is found to be applicable in a certain parameter range, which is in good agreement with the predictions of other methods. As soon as the difference between the stiffness properties of the face sheets and the core of the sandwich increases above a certain threshold, the equivalent single layer loses its validity.

To take more complex deformation modes into account, a continuum mechanics-based commercially available program, ABAQUS, is utilized. The predictions derived from this program are used as the validation reference for the developed compound beam model presented in chapter 3. Major advantages of the compound beam model are found to be its one-dimensional nature, the simplified mathematical evaluation to a sandwich beam.

We considered the results of the simulation by varying the stiffness parameters of the model. Additionally, the effect of core thickness and stiffness and the number of finite elements of the domain discretization used in FEM are examined.

6.1. Future aspects of the work:

One major finding of this work is the accuracy of the proposed linear methods on par with the linear predictions of the ABAQUS. To further extend this method, several suggestions can be considered:

- The deformations of the rubber core can be analyzed in more detail using the asymptotic method to see how it behaves under the conditions presented in this work.
- Deployment of the model for complex structures such as cylinders or anisotropic materials.
- Using numerical models such as the generalized differential quadrature (GDQ) and variational differential quadrature (VDQ), in order to solve the functionals and weak forms.

- Coupled thermally induced deformations.
- Study of rapid heating effects using compound beam model in small time increments.

Bibliography

[1] Vinson, J. The behavior of sandwich structures of isotropic and composite materials. Routledge. (2018).

[2] Hu, H., Belouettar, S., & Potier-Ferry, M. Review and assessment of various theories for modeling sandwich composites. Composite Structures, 84(3), 282-292. (2008).

[3] Ha, K. H. Finite element analysis of sandwich plates: an overview. Computers & Structures, 37(4), pp. 397-403, 1990.

[4] Hemmatian, H. Sandwich panel optimization based on yielding and buckling criteria by using imperialist competitive algorithm. Modares Mechanical Engineering, 13(4), pp. 25-35, 2013.

[5] Pirmohammad, N., Liaght, G. H., & Pol, M. H. Experimental investigation on ballistic behavior of sandwich panels made of honeycomb core. Modares Mechanical Engineering, 14(4), pp. 21-26, 2014.

[6] Frostig, Y., Baruch, M., Vilnay, O., & Sheinman, I. Bending of nonsymmetric sandwich beams with transversely flexible core. *Journal of engineering mechanics*, *117*(9), pp. 1931-1952, 1991.

[7] Frostig, Y. Elastica of sandwich panels with a transversely flexible core—A high-order theory approach. *International Journal of Solids and Structures*, *46*(10), pp. 2043-2059, 2009.

[8] Frostig, Y., & Thomsen, O. T. High-order free vibration of sandwich panels with a flexible core. *International Journal of Solids and Structures*, *41*(5-6), pp.1697-1724, 2004.

[9] Frostig, Y., & Thomsen, O. T. Thermal buckling and postbuckling of sandwich panels with a transversely flexible core. *AIAA journal*, *46*(8), pp. 1976-1989, 2008.

[10] Phan, C. N., Kardomateas, G. A., & Frostig, Y. Blast response of a sandwich beam/wide plate based on the extended high-order sandwich panel theory and comparison with elasticity. *Journal of Applied Mechanics*, *80*(6), 2013.

[11] Jam, J. E., Eftari, B., & Taghavian, S. H. A new improved high-order theory for analysis of free vibration of sandwich panels. *Polymer Composites*, *31*(12), pp. 2042-2048, 2010.

[12] Schwarts-Givli, H., Rabinovitch, O., & Frostig, Y. Free vibration of delaminated unidirectional sandwich panels with a transversely flexible core and general boundary conditions—A high-order approach. *Journal of Sandwich Structures & Materials*, *10*(2), pp. 99-131, 2008.

[13] Phan, C. N., Frostig, Y., & Kardomateas, G. A. Analysis of sandwich beams with a compliant core and with in-plane rigidity—extended high-order sandwich panel theory versus elasticity. Journal of Applied Mechanics, pp. 79(4), 2012.

[14] Frostig, Y., & Thomsen, O. T. Thermal buckling and postbuckling of sandwich panels with a transversely flexible core. AIAA journal, 46(8), pp. 1976-1989, 2008.

[15] Frostig, Y., & Thomsen, O. T. Non-linear thermo-mechanical behaviour of delaminated curved sandwich panels with a compliant core. International Journal of Solids and Structures, 48(14-15), pp. 2218-2237, 2011.

[16] Schwarts-Givli, H., Rabinovitch, O., & Frostig, Y. High-order nonlinear contact effects in cyclic loading of delaminated sandwich panels. *Composites Part B: Engineering*, *38*(1), pp. 86-101, 2007.

[17] Frostig, Y., Thomsen, O. T., & Sheinman, I. On the non-linear high-order theory of unidirectional sandwich panels with a transversely flexible core. International Journal of Solids and Structures, 42(5-6), pp. 1443-1463, 2005.

[18] Hohe, J., & Librescu, L. A nonlinear theory for doubly curved anisotropic sandwich shells with transversely compressible core. International Journal of Solids and Structures, 40(5), pp. 1059-1088, 2003.

[19] Taheri-Behrooz, F., & Mansouri Nik, M. Experimental and numerical analysis of sandwich composite beams under four-point bending. Modares Mechanical Engineering, 17(1), pp. 241-252, 2017.

[20] Kidane, S., Li, G., Helms, J., Pang, S. S., & Woldesenbet, E. Buckling load analysis of grid stiffened composite cylinders. Composites Part B: Engineering, 34(1), pp. 1-9, 2003.

[21] Birman, V., & Kardomateas, G. A. Review of current trends in research and applications of sandwich structures. Composites Part B: Engineering, 142, pp. 221-240, 2018.

[22] Carrera, E., & Brischetto, S. A survey with numerical assessment of classical and refined theories for the analysis of sandwich plates. Applied mechanics reviews, 62(1), 2009.

[23] HOHE, J., & LIBRESCU, L. Advances in the structural modeling of elastic sandwich panels. Mechanics of Advanced Materials and Structures, 11(4-5), pp. 395-424, 2004.

[24] Burton, W. S., & Noor, A. K. Assessment of computational models for sandwich panels and shells. Computer methods in applied mechanics and engineering, 124(1-2), pp. 125-151, 1995.

[25] Sayyad, A. S., & Ghugal, Y. M. Bending, buckling and free vibration of laminated composite and sandwich beams: A critical review of literature. Composite Structures, 171, pp. 486-504, 2017.

[26] Reddy, J. N. Mechanics of laminated composite plates and shells: theory and analysis. CRC press, 2003.

[27] Abrate, S., & Di Sciuva, M. Equivalent single layer theories for composite and sandwich structures: A review. Composite Structures, 179, pp. 482-494, 2017.

[28] Barut, A., Madenci, E., Anderson, T., & Tessler, A. Equivalent single-layer theory for a complete stress field in sandwich panels under arbitrarily distributed loading. Composite Structures, 58(4), pp. 483-495, 2002.

[29] Skvortsov, V., & Bozhevolnaya, E. Two-dimensional analysis of shallow sandwich panels. Composite structures, 53(1), pp. 43-53, 2001.

[30] Karttunen, A. T., Reddy, J. N., & Romanoff, J. Micropolar modeling approach for periodic sandwich beams. Composite Structures, 185, pp. 656-664, 2018.

[31] Eringen, A. C., & Suhubi, E. S. Nonlinear theory of simple micro-elastic solids—I. International Journal of Engineering Science, 2(2), pp. 189-203, 1964.

[32] Li, L., & Xie, S. Finite element method for linear micropolar elasticity and numerical study of some scale effects phenomena in MEMS. International Journal of Mechanical Sciences, 46(11), pp. 1571-1587, 2004.

[33] Pothier, A., & Rencis, J. J. Three-dimensional finite element formulation for microelastic solids. Computers & structures, 51(1), pp. 1-21, 1994.

[34] Kvasov, R., & Steinberg, L. Numerical modeling of bending of micropolar plates. Thin-Walled Structures, 69, pp. 67-78, 2013.

[35] Zhou, X., & Cusatis, G. Tetrahedral finite element with rotational degrees of freedom for Cosserat and Cauchy continuum problems. Journal of Engineering Mechanics, 141(2), 06014017, 2015.

[36] Ansari, R., Norouzzadeh, A., Shakouri, A. H., Bazdid-Vahdati, M., & Rouhi, H. Finite element analysis of vibrating micro-beams and-plates using a three-dimensional micropolar element. Thin-Walled Structures, 124, pp. 489-500, 2018.

[37] Ansari, R., Shakouri, A. H., Bazdid-Vahdati, M., Norouzzadeh, A., & Rouhi, H. A nonclassical finite element approach for the nonlinear analysis of micropolar plates. Journal of Computational and Nonlinear Dynamics, 12(1), 2017.

[38] Godio, M., Stefanou, I., Sab, K., & Sulem, J. Dynamic finite element formulation for Cosserat elastic plates. International Journal for Numerical Methods in Engineering, 101(13), pp. 992-1018, 2015.

[39] Huang, F. Y., Yan, B. H., Yan, J. L., & Yang, D. U. Bending analysis of micropolar elastic beam using a 3-D finite element method. International journal of engineering science, 38(3), pp. 275-286, 2000.

[40] Hassanpour, S., & Heppler, G. Uncomplicated torsion and bending theories for micropolar elastic beams. In Proceedings of the 11th World Congress on Computational Mechanics. Barcelona, Spain, 2014.

[41] Regueiro, R. A., & Duan, Z. Static and dynamic micropolar linear elastic beam finite element formulation, implementation, and analysis. Journal of Engineering Mechanics, 141(8), 04015026, 2015.

[42] Bauchau, O. A., & Craig, J. I. Kirchhoff plate theory. In *Structural analysis* (pp. 819-914). Springer, Dordrecht, 2009

[43] Mindlin, R. D. Influence of rotatory inertia and shear on flexural motions of isotropic, elastic plates, 1951.

[44] Reissner, E., & Stavsky, Y. Bending and stretching of certain types of heterogeneous aeolotropic elastic plates, 1961.

[45] Whitney, J. M., & Pagano, N. J. Shear deformation in heterogeneous anisotropic plates, 1970.

[46] Di Sciuva, M. Bending, vibration and buckling of simply supported thick multilayered orthotropic plates: an evaluation of a new displacement model. Journal of Sound and Vibration, 105(3), pp. 425-442, 1986.

[47] Birman, V., & Bert, C. W. On the choice of shear correction factor in sandwich structures. *Journal of Sandwich Structures & Materials*, *4*(1), pp. 83-95, 2002.

[48] Reissner, E. Reflections on the theory of elastic plates, 1985.

[49] Librescu, L., Khdeir, A. A., & Reddy, J. N. A comprehensive analysis of the state of stress of elastic anisotropic flat plates using refined theories. *Acta Mechanica*, *70*(1), pp. 57-81, 1987.

[50] Noor, A. K., & Burton, W. S. Assessment of shear deformation theories for multilayered composite plates, 1989.

[51] Reddy, J. N. A simple higher-order theory for laminated composite plates, 1984.

[52] Vetyukov, Yury. Nonlinear mechanics of thin-walled structures: asymptotics, direct approach and numerical analysis. Springer Science & Business Media, 2014.

[53] Antman, S. Kirchhoff's problem for nonlinearly elastic rods. Quarterly of applied mathematics, 32(3), pp. 221-240, 1974.

[54] " Mechanics of Composite Materials: Lecture 8-1st Order Shear Deformation Theory (Sandwich Plates)" YouTube, Apr.25.2020 [Video file]. Available: https://youtu.be/-h2N-iWQFtQ. [Accessed: Apr.2021].